AD-A125 203

NAVAL OCEAN SYSTEMS CENTER, SAN DIEGO, CA
ANALYSIS OF ELECTROMAGNETIC PROPERTIES OF THE GROUND STAKE ANTENNA PREPARED BY CM BUTLER, CA HARRISON, AND AW GLISSON, Jr. DEPARTMENT OF ELECTRICAL ENGINEERING UNIVERSITY OF MISSISSIPPI

1 OF 1
CR 146
UNCLS
31 AUG 1982

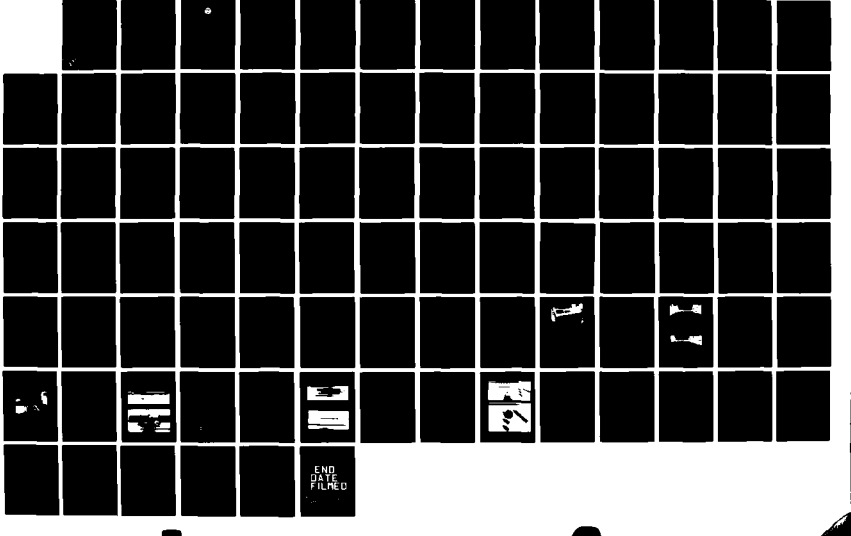

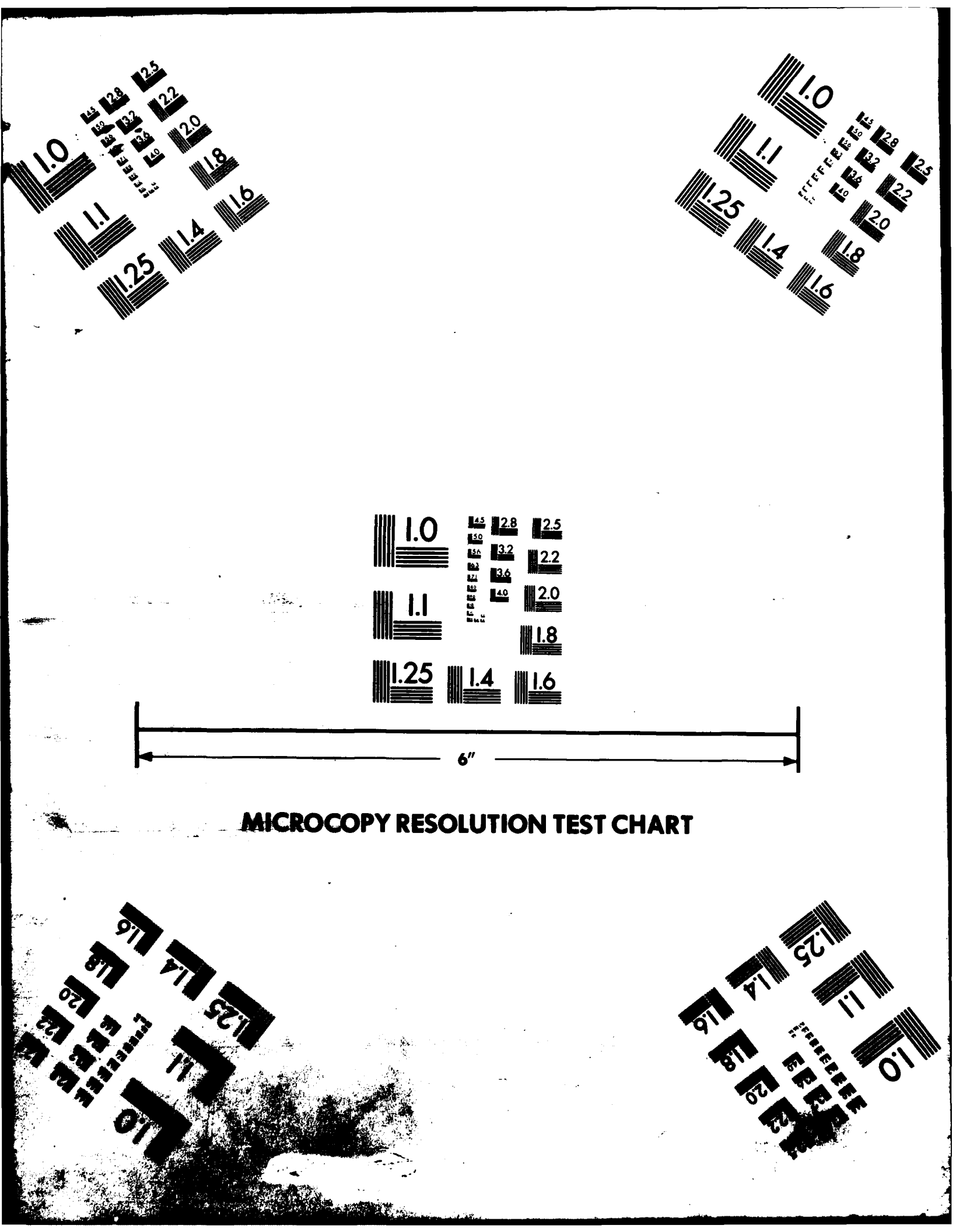

MICROCOPY RESOLUTION TEST CHART

NOSC CR 146

Contractor Report 146

ANALYSIS OF ELECTROMAGNETIC PROPERTIES OF THE GROUND STAKE ANTENNA

Prepared by
CM Butler, CA Harrison, and AW Glisson, Jr
Department of Electrical Engineering
University of Mississippi

31 August 1982

Interim Technical Report for Period 15 March-31 August 1982

Prepared for
NOSC Code 811

Sponsored by
Naval Electronic Systems Command
PME 110-241
and
US Army CEEIA
Fort Huachuca AZ

NAVAL OCEAN SYSTEMS CENTER
San Diego, California 92152

NAVAL OCEAN SYSTEMS CENTER, SAN DIEGO, CA 92152

AN ACTIVITY OF THE NAVAL MATERIAL COMMAND

JM PATTON, CAPT, USN
Commander

HL BLOOD
Technical Director

ADMINISTRATIVE INFORMATION

Work was performed under Contract N66001-82-C-0045 by CM Butler, CA Harrison, and AW Glisson, Jr, of the Department of Electrical Engineering, University of Mississippi, University MS 38677, for NOSC Communications Research and Technology Division, Code 811. It was sponsored jointly by Naval Electronic Systems Command, PME 110-241, and US Army CEEIA, Fort Huachuca AZ, and was monitored by NOSC under program element 11402N (NOSC 811-CM35). This interim report covers work from 15 March to 31 August 1982 and was approved for publication 31 August 1982.

Released by
MS Kvigne, Head
Communications Research
and Technology Division

Under authority of
HD Smith, Head
Communications Systems
and Technology Department

UNCLASSIFIED

SECURITY CLASSIFICATION OF THIS PAGE (When Data Entered)

REPORT DOCUMENTATION PAGE		READ INSTRUCTIONS BEFORE COMPLETING FORM
1. REPORT NUMBER NOSC Contractor Report 146 (CR 146)	2. GOVT ACCESSION NO.	3. RECIPIENT'S CATALOG NUMBER
4. TITLE (and Subtitle) ANALYSIS OF ELECTROMAGNETIC PROPERTIES OF THE GROUND STAKE ANTENNA		5. TYPE OF REPORT & PERIOD COVERED Interim Technical 15 March–31 August 1982 6. PERFORMING ORG. REPORT NUMBER
7. AUTHOR(s) CM Butler CA Harrison AW Glisson, Jr		8. CONTRACT OR GRANT NUMBER(s) N66001-82-C-0045
9. PERFORMING ORGANIZATION NAME AND ADDRESS Department of Electrical Engineering University of Mississippi University MS 38677		10. PROGRAM ELEMENT, PROJECT, TASK AREA & WORK UNIT NUMBERS PE 11402N (NOSC 811-CM35)
11. CONTROLLING OFFICE NAME AND ADDRESS Naval Electronic Systems Command, PME 110-241, Washington DC 20360; US Army CEEIA, Fort Huachuca AZ 85613		12. REPORT DATE 31 August 1982 13. NUMBER OF PAGES 85
14. MONITORING AGENCY NAME & ADDRESS(if different from Controlling Office) Naval Ocean Systems Center San Diego CA 92152		15. SECURITY CLASS. (of this report) Unclassified 15a. DECLASSIFICATION/DOWNGRADING SCHEDULE

16. DISTRIBUTION STATEMENT (of this Report)

Approved for public release; distribution unlimited.

17. DISTRIBUTION STATEMENT (of the abstract entered in Block 20, if different from Report)

18. SUPPLEMENTARY NOTES

19. KEY WORDS (Continue on reverse side if necessary and identify by block number)

Electromagnetic fields and waves
Microwave measurements
Monopole antenna
Antenna above water
Antenna in two-media space

20. ABSTRACT (Continue on reverse side if necessary and identify by block number)

In this interim technical report is described progress to date in the following facets of an investigation of the electromagnetic properties of the so-called ground stake antenna: *(i)* formulation and numerical analysis of integral equations for the problem of determining the characteristics of a coax-fed monopole antenna in a lossy medium, *(ii)* formulation of the integral equation for a cylindrical antenna which resides in two contiguous half spaces, and *(iii)* development of the measurement apparatus and techniques for the experimental investigation of the properties of a cylindrical antenna which resides in two contiguous half spaces. The report focuses upon the

(Continued on reverse side)

DD FORM 1 JAN 73 1473 EDITION OF 1 NOV 65 IS OBSOLETE

S/N 0102-LF-014-6601

UNCLASSIFIED

SECURITY CLASSIFICATION OF THIS PAGE (When Data Entered)

20. Continued.
derivations of integral equations and the development of associated analytical/numerical techniques needed to solve them efficiently, as well as upon the construction of experimental apparatus and refinement of measurement schemes needed to collect data for corroboration of results obtained from the integral equation solutions.

TABLE OF CONTENTS

LIST OF FIGURES

1. INTRODUCTION

This is an interim technical report in which is outlined the accomplishments obtained to date by the Department of Electrical Engineering, University of Mississippi, in an investigation of the electromagnetic properties of the so-called ground stake antenna undertaken for the Naval Ocean Systems Center under contract N66001-82-C-0045. The report describes progress made to date in three facets of the overall research project: (*i*) formulation and numerical analysis of integral equations for the problem of determining the characteristics of a coax-fed monopole antenna in a lossy medium, (*ii*) formulation of the integral equation for a cylindrical antenna which resides in two contiguous half spaces, and (*iii*) development of the measurement apparatus and techniques for the experimental investigation of the properties of a cylindrical antenna which resides in two contiguous half spaces.

In Section 2 is presented a detail discussion of the derivation of the coupled integral equations for a monopole in a lossy medium that is fed by a coaxial waveguide through a ground plane. The equations involve integrals whose integrands are singular and infinite series whose terms contain Bessel functions, so to solve these equations numerically requires great care. Therefore, in this section several analyses are described that enable one to render all terms in the equations amenable to efficient and accurate numerical computations.

Section 3 is devoted to a description of the formulation of the integral equation for the ground stake antenna. Because the ground stake cylindrical antenna is partially in one medium and partially in another.

Sommerfeld integrals are incorporated in Green's functions which appear in the integral equation. At best, Sommerfeld integrals are difficult to evaluate efficiently and accurately so significant attention is given to the developemnt of equations in a form that can be solved numerically with high efficiency. As opposed to double integration which one must confront in the Green's functions for the ground stake antenna when one derives these Green's functions from the traditional Sommerfeld integrals for an elementary dipole, it has been possible by taking a fresh approach to obtain Green's functions possessing only single integrals. A brief study of this integral equation reveals that it can be solved numerically rather readily.

In Section 4 is found a detailed description of the apparatus and procedures presently under development for experimentally studying the properties of the ground stake antenna. Construction details of the tank in which the antenna is to be placed for measurements are presented. Also, the various pieces of apparatus that have been constructed for the measurement of the properties of water are described. Finally, the measurement techniques to be employed are outlined briefly.

2. FORMULATION AND ANALYTICAL/NUMERICAL PROCESSING OF COUPLED INTEGRAL EQUATIONS FOR COAX-FED MONOPOLE ABOVE A GROUND PLANE

In this section is found a derivation and an analysis of the coupled integral equations for a coax-fed monopole above a ground plane (Fig. 1). The monopole resides in a lossy medium of infinite extent. These equations and the numerical techniques developed for solving them provide the basis upon which one may found an accurate analysis of an antenna in a lossy medium.

The monopole antenna illustrated in Fig. 1 is the extension of the center conductor of a coaxial waveguide whose outer conductor terminates at the conducting ground plane. The monopole is taken to be a conducting tube (open-ended) with a vanishingly thin wall. It is fed or driven by a time-harmonic signal ($e^{j\omega t}$) from the coaxial guide and receives its excitation through the annular aperture where the coax opens into the ground plane. The monopole is of height h and radius Λ and it resides in a semi-infinite, homogeneous medium characterized by (μ,ε) with ε $(= \varepsilon_0\varepsilon_r - j\frac{\sigma}{\omega})$ allowed to be complex to account for losses. The radii of the inner and outer coax conductors are a and b, respectively, and the medium in the annular region between the conductors may be uniform in which case it is characterized by (μ_c,ε_c) or it may be a gas (μ_g,ε_g) in which a dielectric (μ_c,ε_c) bead of length L is inserted to provide mechanical support. (See Fig. 2 .) In the former case of a uniform solid dielectric, L is made to approach infinity. As suggested in Fig. 2 , the monopole radius may differ from that of the coax inner conductor.

We wish to calculate the current induced in the monopole and to determine the load, or admittance, which the monopole presents to the

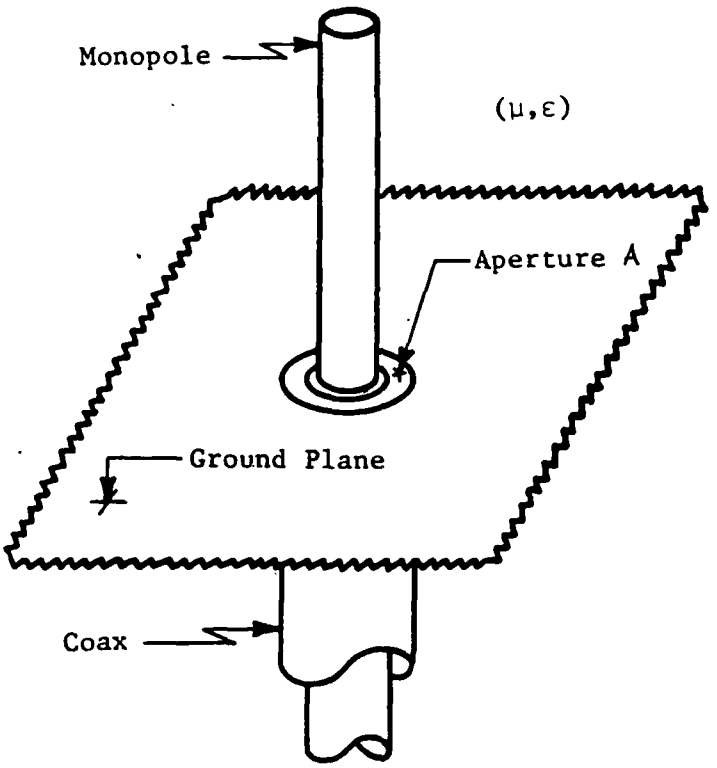

Fig. 1. Coax-fed monopole above a ground plane.

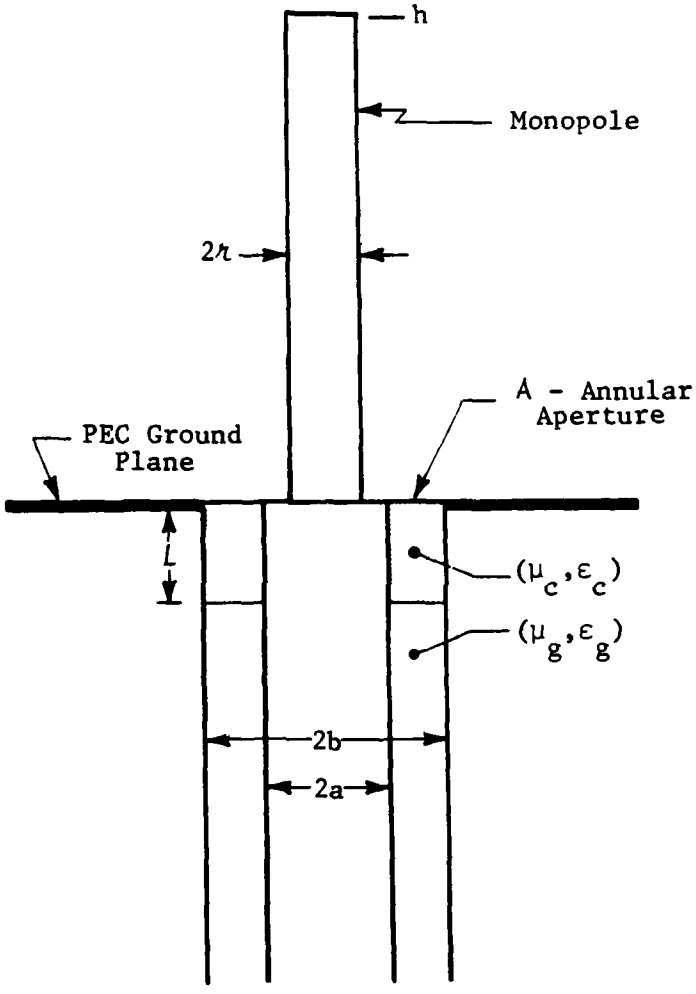

Fig. 2. Cross-section of coax-fed monopole above a ground plane (for coax filled with uniform solid dielectric, $L \to \infty$).

coaxial line. The known excitation is specified to be a TEM wave traveling in the positive z direction in the coax, whose field components are

$$E_\rho^i = \frac{E_0}{\rho} e^{-jk_c z}, \quad H_\phi^i = \frac{E_0}{\eta_c \rho} e^{-jk_c z}, \tag{1}$$

where $k_c^2 = \omega^2 \mu_c \varepsilon_c$ and $\eta_c^2 = \mu_c/\varepsilon_c$ and where E_0 is the known complex amplitude of the TEM electric field incident upon the annular aperture. If the coax is gas-filled and the center conductor is supported by a dielectric bead, k_c and η_c are replaced by k_g and η_g, respectively. The viewpoint taken here is that the monopole can be treated as a scatterer which is illuminated by the field radiated by the coaxial aperture in the screen. This approach enables us to apply aperture and scattering theory to the present analysis and provides the basis for the formulation of a pair of coupled integral equations for the monopole-coax structure. As an aid in the derivation of equations, the formulation is partitioned into three parts: field in coaxial region, field radiated by annular aperture, field scattered by monopole.

Formulation of Integral Equations

Coupled integral equations are formulated in this section for the unknowns I and E_ρ^a where I is the total axial current on the monopole and E_ρ^a is the ρ component of the electric field in the annular aperture A through which the coaxial guide and monopole antenna are coupled. These integral equations are derived by requiring (*i*) that the ϕ component of the H-field in the coax be equal to that in the exterior region when both are evaluated in the limit as the points of observation approach the annular aperture and (*ii*) that the electric field tangential to the monopole and to the conducting plane be zero. For this purpose the

magnetic field is expressed in the coaxial guide as a function of E_ρ^a and of the excitation and in the exterior region as a function of E_ρ^a and I.

Magnetic Field in Coaxial Guide

The magnetic field H_ϕ^{co} in the coaxial guide can be written in terms of the coax excitation of (1) and aperture field E_ρ^a as

$$H_\phi^{co}(\rho,z) = H_\phi^{sc}(\rho,z) + H_\phi^{c}(\rho,z) \tag{2a}$$

where

$$H_\phi^{c}(\rho,z) = \int_a^b E_\rho^a(\rho')G^c(\rho,z;\rho')d\rho' \tag{2b}$$

and in which

$$H_\phi^{sc}(\rho,z) = 2\,\frac{E_0}{\eta_c \rho}\cos k_c z \tag{3a}$$

is the so-called short-circuit magnetic field which would exist in the uniform-dielectric coax if the aperture at $z = 0$ between the coaxial guide and the exterior region were short-circuited. If the coax is gas-filled with a bead-supported center conductor, the short-circuit magnetic field in the region $-L < z < 0$ would be

$$H_\phi^{sc}(\rho,z) = 2\,\frac{E_0}{\rho}\cdot\frac{e^{jk_g L}}{\eta_g \cos k_c L + j\,\eta_c \sin k_c L}\cos k_c z,\ z\ \varepsilon(-L,0). \tag{3b}$$

In the case of the gas-filled coax, (2a) is valid only in the bead material ($-L < z < 0$), and it is assumed that higher order modes excited at the discontinuity at $z = 0$ are vanishing small at $z = -L$. The

Green's function G^c is determined by standard methods [1] to be

$$G^c(\rho,z;\rho') = -\frac{1}{\eta_c \rho \ell n\frac{b}{a}} e^{jk_c z}\left[\frac{1-\Gamma e^{-j2k_c(z+L)}}{1+\Gamma e^{-j2k_c L}}\right]$$

$$-\frac{k_c}{\eta_c}\rho' \sum_{q=1}^{\infty} \frac{1}{\chi_q N_q^2}\frac{d}{d\rho'}\Phi_q(\rho')\frac{d}{d\rho}\Phi_q(\rho)\, e^{j\chi_q z} \qquad (4)$$

$$z\varepsilon(-L,0)$$

where

$$\Gamma = \frac{\eta_g - \eta_c}{\eta_g + \eta_c} \quad , \qquad (5)$$

where

$$\Phi_q(\rho) = N_0(k_{tq}a)\, J_0(k_{tq}\rho) - J_0(k_{tq}a)\, N_0(k_{tq}\rho) \quad , \qquad (6)$$

and where

$$\chi_q = \begin{cases} \sqrt{k_c^2 - k_{tq}^2} & , \; k_{tq}^2 < k_c^2 \\ -j\sqrt{k_{tq}^2 - k_c^2} & , \; k_{tq}^2 > k_c^2 \end{cases} \qquad (7)$$

in which k_{tq}, $q = 1,2,\ldots,$ is the q^{th} root of $\Phi_b(b) = 0$. In (6), J_ν and N_ν are the ν^{th} order Bessel and Neumann functions and the norm N_q^2 in (4) is

$$N_q^2 = \int_a^b \rho\left[\frac{d}{d\rho}\Phi_q(\rho)\right]^2 d\rho = \frac{b^2}{2}\left(\left[\frac{d}{d\rho}\Phi_q(\rho)\right]_{\rho=b}\right)^2 - \frac{2}{\pi^2} \quad . \qquad (8)$$

The Green's function G^c of (4) is valid for both the uniform-dielectric coax and the gas-filled coax with bead-supported center conductor; in the former case, Γ is set equal to zero in the first term of (4).

Field in Exterior Region

The magnetic field in the exterior region is determined as the sum

$$H_\phi^{ex} = H_\phi^r + H_\phi^s \tag{9}$$

where H_ϕ^r is that radiated by the annular aperture in the absence of the monopole and H_ϕ^s is that scattered by the monopole. The field incident upon the monopole is that radiated by the aperture. As an aid in deriving expressions for the exterior field, the exterior-field equivalent model of Fig. 3 is introduced. In this figure one sees that the annular aperture A at $z = 0$ is short-circuited and that an equivalent surface magnetic current of density $\underline{M} = M_\phi \hat{\underline{\phi}}$ where $M_\phi = \hat{\underline{\phi}} \cdot \left[E_\rho^a \, \hat{\underline{\rho}} \times \hat{\underline{z}} \right]$ or $M_\phi = -E_\rho^a$ is placed on the shorted annulus [2]. This model and its field are equivalent to the original structure and its field in the exterior ($z > 0$) region [2]. By image theory one arrives at the final model of Fig. 3 which is used as a guide in exterior formulations.

In the absence of the monopole, the field $(\underline{E}^r, \underline{H}^r)$ due to the magnetic current is determined from

$$\underline{E}^r = -\frac{1}{\varepsilon} \nabla \times \underline{F} \tag{10a}$$

and

$$\underline{H}^r = -j \frac{\omega}{k^2} (k^2 \underline{F} + \nabla\nabla \cdot \underline{F}) \tag{10b}$$

where

$$\underline{F}(\underline{r}) = \frac{\varepsilon}{4\pi} \iint_A 2M_\phi(\underline{\rho}') \hat{\underline{\phi}}' \frac{e^{-jk|\underline{r}-\underline{\rho}'|}}{|\underline{r}-\underline{\rho}'|} \, dS' \tag{11}$$

or where $\underline{F} = F_\phi \hat{\underline{\phi}}$ with

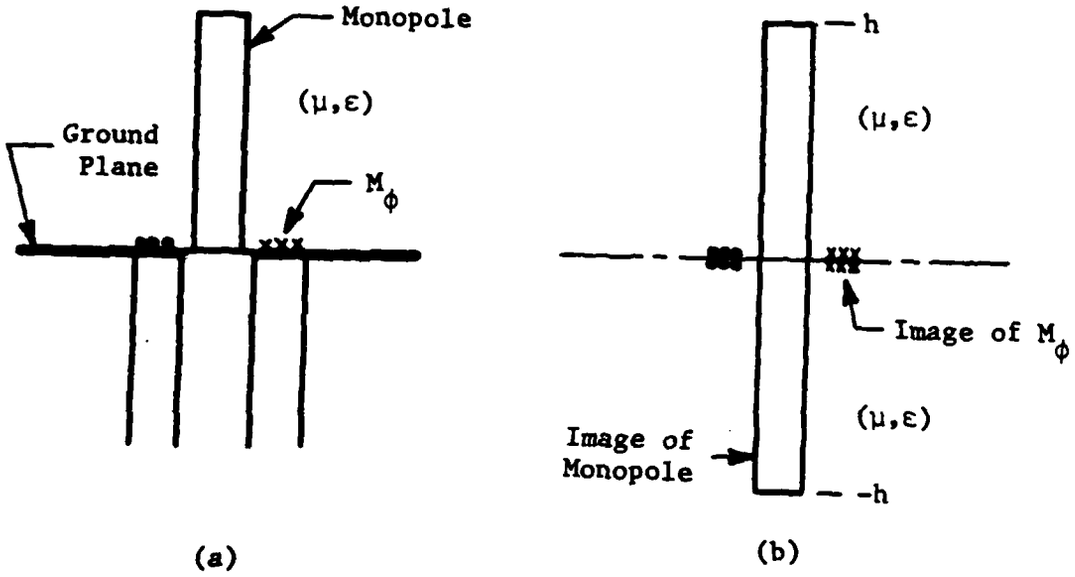

Fig. 3. Exterior-region equivalent models of coax-fed monopole.

$$F_\phi(\rho,z) = -\frac{\varepsilon}{2\pi}\int_a^b \rho' E_\rho^a(\rho') \int_{-\pi}^{\pi} \cos\phi' \frac{e^{-jk[z^2+R^2]^{\frac{1}{2}}}}{[z^2+R^2]^{\frac{1}{2}}}\, d\phi' d\rho' \qquad (12a)$$

in which $k^2 = \omega^2\mu\varepsilon$ and $\eta^2 = \mu/\varepsilon$ and

$$R^2 = [\rho^2 + \rho'^2 - 2\rho\rho'\cos\phi'] \ . \qquad (12b)$$

From (10) and (12) one readily finds that the field components E_z^r and H_ϕ^r are

$$E_z^r(\rho,z) = \frac{1}{2\pi\rho}\frac{\partial}{\partial\rho}\,\rho\int_a^b \rho' E_\rho^a(\rho') \int_{-\pi}^{\pi} \cos\phi' \frac{e^{-jk[z^2+R^2]^{\frac{1}{2}}}}{[z^2+R^2]^{\frac{1}{2}}}\, d\phi' d\rho' \ . \qquad (13)$$

and

$$H_\phi^r(\rho,z) = j\,\frac{1}{2\pi}\frac{k}{\eta}\int_a^b \rho' E_\rho^a(\rho') \int_{-\pi}^{\pi} \cos\phi' \frac{e^{-jk[z^2+R^2]^{\frac{1}{2}}}}{[z^2+R^2]^{\frac{1}{2}}}\, d\phi' d\rho'. \qquad (14)$$

The field $(\underline{E}^s, \underline{H}^s)$ due to the total axial current I induced on the monopole can be determined from

$$\underline{E}^s = -j\,\frac{\omega}{k^2}\,(k^2\underline{A} + \underline{\nabla\nabla}\cdot\underline{A}) \qquad (15a)$$

and

$$\underline{H}^s = \frac{1}{\mu}\,\underline{\nabla}\times\underline{A} \qquad (15b)$$

where $\underline{A}$ has only a z-component given by

$$A_z(\rho,z) = \frac{\mu}{4\pi}\int_{-h}^{h} I(z')\,\frac{1}{2\pi}\int_{-\pi}^{\pi} \frac{e^{-jk[(z-z')^2+R_\ell^2]^{\frac{1}{2}}}}{[(z-z')^2+R_\ell^2]^{\frac{1}{2}}}\, d\phi' dz' \qquad (16)$$

in which R_ℓ^2 is R^2 of (12b) with ρ' replaced by ℓ. As is consistent with the fact that the excitation of the monopole emanating from the aperture is ϕ independent, the current on the monopole and the resulting scattered field are also ϕ independent. Expressions for the field components E_z^s and H_ϕ^s follow immediately:

$$E_z^s(\rho,z) = -j\frac{\eta}{4\pi k}\left(\frac{d^2}{dz^2}+k^2\right)\int_{-h}^{h} I(z')\frac{1}{2\pi}\int_{-\pi}^{\pi}\frac{e^{-jk[(z-z')^2+R_\ell^2]^{\frac{1}{2}}}}{[(z-z')^2+R_\ell^2]^{\frac{1}{2}}}\,d\phi'dz' \tag{17}$$

$$H_\phi^s(\rho,z) = -\frac{1}{4\pi}\frac{\partial}{\partial\rho}\int_{-h}^{h} I(z')\frac{1}{2\pi}\int_{-\pi}^{\pi}\frac{e^{-jk[(z-z')^2+R_\ell^2]^{\frac{1}{2}}}}{[(z-z')^2+R_\ell^2]^{\frac{1}{2}}}\,d\phi'dz' \; . \tag{18}$$

Integral Equations

The final integral equations for E_ρ^a and I result from enforcement of boundary and transition conditions. The boundary condition is that the total electric field tangential to the monopole and ground plane surfaces be zero. The tangential E-field on the ground plane is zero by virtue of the use of image theory in the construction of expressions for $\underline{E}^r$ and $\underline{E}^s$ and that on the surface of the tubular monopole is made zero by enforcement of the following equation:

$$E_z^s(\ell,z) + E_z^r(\ell,z) = 0 \quad , \; z\varepsilon(-h,h) \; . \tag{19}$$

The required transition condition is that the magnetic field tangential to the annular aperture A in the exterior region and that in the coax be equal when the points of observation approach a common point in A. This condition is ensured upon enforcement of

$$\lim_{z\uparrow 0} H_\phi^{co}(\rho,z) = \lim_{z\downarrow 0} H_\phi^{ex}(\rho,z) \quad , \; \rho\varepsilon A$$

or of

$$\lim_{z\uparrow 0} H_\phi^{co}(\rho,z) = \lim_{z\downarrow 0}\left(H_\phi^r(\rho,z) + H_\phi^s(\rho,z)\right) \quad , \; \rho\varepsilon A \; . \tag{20}$$

Eqs. (19) and (20) must hold simultaneously and, upon utilization of (2), (3), and (13)-(18), they lead to the coupled integral equations

below for E_ρ^a and I:

$$-j\frac{\eta}{4\pi k}\left(\frac{d^2}{dz^2}+k^2\right)\int_{-h}^{h} I(z')\,G^s(\rho,z;z')dz'$$

$$+\frac{1}{\rho}\left[\frac{\partial}{\partial\rho}\,\rho\int_a^b \rho' E_\rho^a(\rho')\,G^a(\rho,z;\rho')d\rho'\right]_{\rho=\rho} = 0\ ,\ z\varepsilon(-h,h) \qquad (21a)$$

and

$$-\frac{1}{4\pi}\frac{\partial}{\partial\rho}\int_{-h}^{h} I(z')\,G^s(\rho,0;z')dz' + j\frac{k}{\eta}\int_a^b \rho' E_\rho^a(\rho')\,G^a(\rho,0;\rho')d\rho'$$

$$-\int_a^b E_\rho^a(\rho')\,G^c(\rho,0;\rho')d\rho' = H_\phi^{sc}(\rho,0),\ \rho\varepsilon(a,b) \qquad (21b)$$

in which

$$G^s(\rho,z;z') = \frac{1}{2\pi}\int_{-\pi}^{\pi}\frac{e^{-jk[(z-z')^2+R_\rho^2]^{1/2}}}{[(z-z')^2+R_\rho^2]^{1/2}}\,d\phi' \qquad (22a)$$

and

$$G^a(\rho,z;\rho') = \frac{1}{2\pi}\int_{-\pi}^{\pi}\cos\phi'\,\frac{e^{-jk[z^2+R^2]^{1/2}}}{[z^2+R^2]^{1/2}}\,d\phi' \ . \qquad (22b)$$

For subsequent convenience, the integral equations are written below in operator form:

$$E_z^s[I;z] + E_z^r[E_\rho^a;z] = 0\ ,\ z\varepsilon(-h,h) \qquad (23a)$$

and

$$H_\phi^s[I;\rho] + H_\phi^r[E_\rho^a;\rho] - H_\phi^c[E_\rho^a;\rho] = H_\phi^{sc}(\rho,0)\ ,\ \rho\varepsilon(a,b)\ . \qquad (23b)$$

I and $E_\rho^a(=-M_\phi)$ can be determined by solving the coupled integral equations and from knowledge of these two quantities the radiated field and the input TEM reflection coefficient of the coaxial guide can be computed.

Numerical Solution of Coupled Integral Equations

The integral equations for E_ρ^a and I are far too complex to be solved by any but a well-conceived numerical method. Due to the presence of G^c, one must sum an infinite series comprising terms involving derivatives of Φ_q which depends upon Bessel and Neumann functions whose arguments are determined by a solution of a transcendental equation for each q. In addition the following terms in the integral equations involve integrals whose integrands may be singular: $E_z^s(\ell,z)$, $E_z^r(\ell,z)$, $\lim_{z\downarrow 0} H_\phi^c(\rho,z)$, and $\lim_{z\downarrow 0} H_\phi^{ex}(\rho,z)$. A technique has been developed for solving numerically the integral equations and schemes to handle all the difficulties enumerated have been devised. This technique is described below.

The current I on the monopole and its image as well as ρE_ρ^a in the annulus are represented by linear combinations of pulses Π_n of the forms

$$I(z) = \sum_{n=1}^{N_s} I_n \Pi_n(z) \tag{24a}$$

and

$$\rho E_\rho^a(\rho) = \sum_{n=1}^{N_a} V_n \Pi_n(\rho) \tag{24b}$$

where I_n and V_n are unknown constants to be determined, N_s is the number of non-zero pulses in the interval (-h,h), and N_a is the number of pulses in the interval (a,b). The pulse functions are defined as

$$\Pi_n(\zeta) = \begin{cases} 1, & \zeta \in (\zeta_n - \Delta\zeta/2,\ \zeta_n + \Delta\zeta/2) \\ \\ 0, & \text{otherwise} \end{cases} \tag{25}$$

where ζ_n is the pulse center and $\Delta\zeta$ is its width. On (-h,h) the n^{th} pulse center is at $z_n = -h + n\Delta z$ and the pulse width Δz has value $\Delta z = 2h/(N_s+1)$ while on (a,b) the n^{th} pulse center is at $\rho_n = a + \Delta\rho(n-\frac{1}{2})$ and the pulse width $\Delta\rho$ has value $\Delta\rho = (b-a)/N_a$. In keeping with the boundary condition $I(\pm h) = 0$, "half pulses" are placed on the subintervals $(-h,-h+\Delta z/2)$ and $(h-\Delta z/2,h)$, and their coefficients are set equal to zero. Eq. (21a) is tested [3] with triangles Λ_m, $m = 1,\ldots,N_s$, defined by

$$\Lambda_m(z) = \begin{cases} 1 - \dfrac{|z - z_m|}{\Delta z}, & z\varepsilon(z_{m-1}, z_{m+1}) \\ \\ 0, & \text{otherwise} \end{cases} \tag{26}$$

to obtain

$$\sum_{n=1}^{N_s} I_n Z_{mn} + \sum_{n=1}^{N_a} V_n \Gamma_{mn}^{sa} = 0, \quad m=1,2,\ldots,N_s \tag{27a}$$

where

$$Z_{mn} = +j\frac{\eta}{4\pi k}\int_{-h}^{h}\Lambda_m(z)\left(\frac{d^2}{dz^2} + k^2\right)\int_{-h}^{h}\Pi_n(z')\,K(z-z')dz'dz \tag{27b}$$

and

$$\Gamma_{mn}^{sa} = -\frac{1}{\pi}\int_{-h}^{h}\Lambda_m(z)\left[\frac{\partial}{\partial\rho}\,\rho\int_{a}^{b}\Pi_n(\rho')\,G^a(\rho,z;\rho')d\rho'\right]_{\rho=\pi}dz\,. \tag{27c}$$

In (27b) $K(z-z') = G^s(\rho,z;z')$ is the exact kernel [4] of cylindrical antenna and scatterer theory. Eq. (21b) is tested with delta functions or is simply enforced at match point ρ_m located at the centers of pulses to arrive at

$$\sum_{n=1}^{N_s} I_n \Gamma_{mn}^{as} + \sum_{n=1}^{N_a} V_n [Y_{mn} - Y_{mn}^c] = H_m^{sc} \qquad (28a)$$

$$m = 1,2,\ldots,N_a$$

where $H_m^{sc} = H_\phi^{sc}(\rho_m,0)$, where $\rho_m = a + \Delta\rho(m-\frac{1}{2})$, and where

$$\Gamma_{mn}^{as} = -\frac{1}{4\pi}\left[\frac{\partial}{\partial\rho}\int_{-h}^{h} \Pi_n(z')\, G^s(\rho,0;z')dz'\right]_{\rho=\rho_m} , \qquad (28b)$$

$$Y_{mn} = j\frac{k}{\eta}\int_a^b \Pi_n(\rho')\, G^a(\rho_m,0;\rho')d\rho' , \qquad (28c)$$

and

$$Y_{mn}^c = \int_a^b \Pi_n(\rho')\,\frac{1}{\rho'}\, G^c(\rho_m,0;\rho')d\rho' . \qquad (28d)$$

In view of the properties of the pulse function Π_n of (25) and of the triangle function Λ_m of (26), Z_{mn} and Γ_{mn}^{sa} of (27) can be simplified [5 , 6] to

$$Z_{mn} = j\frac{\eta}{4\pi k\Delta z}\int_{-\Delta z/2}^{\Delta z/2}\Big\{K(z_{m+1} - z_n - \zeta) - 2[1-\tfrac{1}{2}(k\Delta z)^2]\, K(z_m - z_n - \zeta)$$

$$+ K(z_{m-1} - z_n - \zeta)\Big\}\, d\zeta \qquad (29a)$$

and

$$\Gamma_{mn}^{sa} = -\frac{1}{h}\int_{-\Delta z}^{\Delta z}[1-|\zeta|/\Delta z]\left[\frac{\partial}{\partial\rho}\,\rho\int_{-\Delta\rho/2}^{\Delta\rho/2}G^{a}(\rho,\ \zeta+z_m;\ \xi+\rho_n)d\xi\right]_{\rho=h}d\zeta\ . \qquad (29b)$$

Integration by parts twice and the change of variable $z' = z_n + \zeta$ are employed to transform (27b) into (29a) while the variable changes $z = z_m + \zeta$ and $\rho' = \rho_n + \xi$ are employed to transform (27c) into (29b). Also involved in the conversion from (27b) to (29a) is a very accurate approximation [5 , 6]. By making use of properties of Π_n and the variable changes mentioned above, the expressions of (28) for Γ_{mn}^{as} , Y_{mn}, and Y_{mn}^{c} can be converted to

$$\Gamma_{mn}^{as} = -\frac{1}{4\pi}\left[\frac{\partial}{\partial\rho}\int_{-\Delta z/2}^{\Delta z/2}G^{s}(\rho,0;z_n+\zeta)d\zeta\right]_{\rho=\rho_m}\ , \qquad (30a)$$

$$Y_{mn} = j\,\frac{k}{\eta}\int_{-\Delta\rho/2}^{\Delta\rho/2}G^{a}(\rho_m,0;\rho_n+\xi)d\xi\ , \qquad (30b)$$

and

$$Y_{mn}^{c} = \int_{-\Delta\rho/2}^{\Delta\rho/2}\frac{1}{\rho_n+\xi}\,G^{c}(\rho_m,0;\rho_n+\xi)d\xi\ . \qquad (30c)$$

To facilitate subsequent discussion it is convenient to express (27a) and (28a) as a single matrix equation of the form

$$\begin{bmatrix}[Z_{mn}] & [\Gamma_{mn}^{sa}]\\ [\Gamma_{mn}^{as}] & [Y_{mn}-Y_{mn}^{c}]\end{bmatrix}\begin{bmatrix}[I_n]\\ [V_n]\end{bmatrix} = \begin{bmatrix}[0]\\ [H_m^{sc}]\end{bmatrix}\ . \qquad (31)$$

Analytical/numerical procedures for computing the matrix elements from (29) and (30) are presented below.

Analytical Aids in the Numerical Evaluation of Matrix Elements

In this section are presented analytical procedures which greatly enhance the accuracy and efficiency of methods for numerical evaluation of the matrix elements of (31). In fact, without the analysis outlined below it is unlikely that sufficient accuracy of matrix element values could be attained to allow acceptable numerical solutions. Z_{mn} is omitted from the discussion below since procedures for its evaluation can be found elsewhere [4,6].

As a first step in casting Γ_{mn}^{sa} into a form suitable for computation we point out that by making use of the analysis presented in [7] one can show that Γ_{mn}^{sa} of (29b) can be reduced to

$$\Gamma_{mn}^{sa} = -\int_{-\Delta z}^{\Delta z} [1-|\zeta|/\Delta z] \int_{-\Delta\rho/2}^{\Delta\rho/2} \frac{\partial}{\partial \xi} G^a(\hbar, \zeta+z_m; \rho_n+\xi) d\xi \, d\zeta$$

$$= -\int_{-\Delta z}^{\Delta z} [1-|\zeta|/\Delta z] \Big[G^a(\hbar, \zeta+z_m; \rho_n+\Delta\rho/2)$$

$$- G^a(\hbar, \zeta+z_m; \rho_n-\Delta\rho/2) \Big] d\zeta \quad . \qquad (32)$$

Evaluation of (32) is essentially the same chore as evaluation of matrix elements in cylindrical antenna/scatterer theory and it can be achieved by methods developed for that purpose. In fact for $n = 1$, $G^a(\hbar, \zeta+z_m; \rho_n-\Delta\rho/2) = G^a(\hbar, \zeta+z_m; a)$ which for $\hbar = a$ is the exact kernel for the circular cylinder, while for $n > 1$ G^a is bounded. Hence, from the

simple expression of (32), one can avail himself of any of the numerous procedures [4 , 6] developed for cylindrical antenna/scatterer theory to evaluate Γ_{mn}^{sa}.

A form of Γ_{mn}^{as} suitable for numerical computation is developed by noting that an interchange of differentiation and integration in (30a) is valid for $\rho \neq a$. Since the bracketed expression in (30a) is evaluated only at points $\rho = \rho_m \geq a + \frac{1}{2}\Delta\rho$, Γ_{mn}^{as} can be rewritten as

$$\Gamma_{mn}^{as} = \frac{1}{8\pi^2} \int_{-h}^{h} \int_{-\pi}^{\pi} \Pi_n(z')(1 + jkD_m)(\rho_m - a\cos\phi') \frac{e^{-jkD_m}}{D_m^3} \, d\phi' dz' \qquad (33)$$

$$\equiv \frac{1}{8\pi^2} \int_{-h}^{h} \int_{-\pi}^{\pi} \Pi_n(z') \, I_{as} \, d\phi' dz'$$

where

$$D_m = [\rho_m^2 + a^2 - 2\rho_m a \cos\phi' + z'^2]^{\frac{1}{2}}.$$

The integrand in (33) is bounded and one can evaluate the integral numerically. Because of the small size of the coax aperture, however, the observation point may be quite near the cylinder surface relative to the length of a source segment on the cylinder. Thus the integrand of (33) may be very highly peaked for the cylinder source segment in which $|z'| < \Delta z/2$. To facilitate evaluation of (33) in this case the integral is expressed in a form more appropriate for numerical calculations. We note that

$$I_{as} \xrightarrow[kD_m \to 0]{} \left(\frac{1}{D_m^3} + \frac{k^2}{2D_m}\right)(\rho_m - a\cos\phi') \equiv I'_{as} \, . \qquad (34)$$

Thus when $n = (N_s+1)/2$, Γ_{mn}^{as} is expressed as

$$\Gamma_{mn}^{as} = \frac{1}{8\pi^2} \int_{\frac{-\Delta z}{2}}^{\frac{\Delta z}{2}} \int_{-\pi}^{\pi} (I_{as} - I'_{as}) d\phi' dz' + \frac{1}{8\pi^2} \int_{\frac{-\Delta z}{2}}^{\frac{\Delta z}{2}} \int_{-\pi}^{\pi} I'_{as} \, d\phi' dz' \, . \qquad (35)$$

The highly peaked behavior of the integrand in (33) is then localized to the integrand of the last integral in (35). Furthermore, integration with respect to the variable z' can be performed analytically on I'_{as} to yield

$$\frac{1}{8\pi^2} \int_{-\pi}^{\pi} \int_{\frac{-\Delta z}{2}}^{\frac{\Delta z}{2}} I'_{as} dz' d\phi' = \frac{1}{8\pi^2} \int_{-\pi}^{\pi} I_{as}^{1'} \, d\phi' + \frac{1}{8\pi^2} \int_{-\pi}^{\pi} I_{as}^{2'} \, d\phi' \qquad (36)$$

where

$$I_{as}^{1'} = \frac{\Delta z[(\rho_m - r) + r(1-\cos\phi')]}{[(\rho_m - r)^2 + 2\rho_m r(1-\cos\phi')][(\rho_m - r)^2 + 2\rho_m r(1-\cos\phi') + (\frac{\Delta z}{2})^2]^{\frac{1}{2}}} \qquad (37a)$$

$$I_{as}^{2'} = k^2(\rho_m - r\cos\phi') \left\{ \ln\left(\frac{\Delta z}{2} + [\rho_m^2 + r^2 - 2\rho_m r\cos\phi' + (\frac{\Delta z}{2})^2]^{\frac{1}{2}} \right) - \frac{1}{2} \ln(\rho_m^2 + r^2 - 2\rho_m r\cos\phi') \right\} \, . \qquad (37b)$$

The integrand $I_{as}^{2'}$ is slowly varying with respect to ϕ' and can be evaluated numerically. The integrand $I_{as}^{1'}$, however, is still highly peaked near $\phi' = 0$. We therefore subtract the small argument behavior

of $I_{as}^{1'}$ under the integral sign and add it to the expression for Γ_{mn}^{as} as a separate integral, so that Γ_{mn}^{as} is finally given by

$$\Gamma_{mn}^{as} = \frac{1}{8\pi^2} \int_{\frac{-\Delta z}{2}}^{\frac{\Delta z}{2}} \int_{-\pi}^{\pi} (I_{as} - I'_{as}) d\phi' dz'$$

$$+ \frac{1}{8\pi^2} \int_{-\pi}^{\pi} (I_{as}^{1'} - I_{as}^{1''}) d\phi' + \frac{1}{8\pi^2} \int_{-\pi}^{\pi} I_{as}^{2'} d\phi'$$

$$+ \frac{1}{8\pi^2} \int_{-\pi}^{\pi} I_{as}^{1''} d\phi' \quad , \; n = (N_s+1)/2 \tag{38}$$

where I_{as}, I'_{as}, $I_{as}^{1'}$, and $I_{as}^{2'}$ are defined in (33)-(37) and where

$$I_{as}^{1''} = \frac{\Delta z[(\rho_m - r) + \frac{1}{2} r\phi'^2]}{[(\rho_m - r)^2 + (\frac{\Delta z}{2})^2]^{\frac{1}{2}}[(\rho_m - r)^2 + \rho_m r\phi'^2]} \tag{39a}$$

$$\int_{-\pi}^{\pi} I_{as}^{1''} \, d\phi' = \frac{\Delta z}{\rho_m[(\rho_m - r)^2 + (\frac{\Delta z}{2})^2]^{\frac{1}{2}}} \left\{ \pi + \frac{\rho_m + r}{\sqrt{\rho_m r}} \tan^{-1}\left(\frac{\pi\sqrt{\rho_m r}}{\rho_m - r} \right) \right\} \tag{39b}$$

For $n \neq (N_s+1)/2$, of course, Γ_{mn}^{as} may be evaluated directly from (33) via numerical integration.

To cast Y_{mn} of (30b) into a form amenable to numerical computation, one first observes from (22b) that the integrand of G^a is unbounded for $m = n$ and that it can be sharply peaked for other combinations of m and n. Thus Y_{mn} must be computed with great care. To this end, we modify the form of this integrand by adding and subtracting $1/R_{mn}$ to obtain

$$\frac{\cos\phi' \, e^{-jkR_{mn}}}{R_{mn}} = \frac{\cos\phi' \, e^{-jkR_{mn}} - 1}{R_{mn}} + \frac{1}{R_{mn}} \tag{40a}$$

where

$$R_{mn}^2 = \rho_m^2 + (\rho_n+\xi)^2 - 2\rho_m(\rho_n+\xi)\cos\phi' \, . \tag{40b}$$

The unboundedness is confined to the second term of (40a) while its first is very slowly varying and can be integrated numerically with ease. Furthermore, the integral over $(-\pi,\pi)$ of the second term can be expressed as

$$\int_{-\pi}^{\pi} \frac{1}{R_{mn}} \, d\phi' = \frac{4}{(\rho_m+\rho_n+\xi)} \int_0^{\pi/2} \frac{1}{\sqrt{1-\beta_{mn}^2 \sin^2\theta}} \, d\theta \tag{41a}$$

$$= \frac{4}{(\rho_m+\rho_n+\xi)} K(\beta_{mn}) \tag{41b}$$

where K is observed to be the complete elliptic integral of the first kind [8] and where

$$\beta_{mn}^2 = 4 \frac{\rho_m(\rho_n+\xi)}{[\rho_m+\rho_n+\xi]^2} \, . \tag{41c}$$

In view of the above, Y_{mn} of (30b) becomes

$$Y_{mn} = j\frac{k}{\eta\pi}\int_{-\Delta\rho/2}^{\Delta\rho/2}\left\{\int_0^{\pi}\left(\frac{\cos\phi' e^{-jkR_{mn}} - 1}{R_{mn}}\right)d\phi' + \frac{2}{(\rho_m+\rho_n+\xi)}K(\beta_{mn})\right\}d\xi. \tag{42}$$

When $m=n$, K is unbounded for $\xi\to 0$ but, fortunately, the small argument form of K can be integrated. That is,

$$\frac{2}{(2\rho_n+\xi)}K(\beta_{nn}) \xrightarrow{\xi\to 0} -\frac{1}{\rho_n}\ln\left(\frac{|\xi|}{8\rho_n}\right) \tag{43}$$

and

$$-\frac{1}{\rho_n}\int_{-\Delta\rho/2}^{\Delta\rho/2}\ln\left(\frac{|\xi|}{8\rho_n}\right)d\xi = \frac{\Delta\rho}{\rho_n}\left[1-\ln\left(\frac{\Delta\rho}{16\rho_n}\right)\right]. \tag{44}$$

Hence, Y_{nn} is

$$\begin{aligned} Y_{nn} = j\frac{k}{\eta\pi}\Bigg\{ & \frac{\Delta\rho}{\rho_n}\left[1-\ln\left(\frac{\Delta\rho}{16\rho_n}\right)\right] \\ & + \int_{-\Delta\rho/2}^{\Delta\rho/2}\left[\frac{2}{(2\rho_n+\xi)}K(\beta_{nn}) + \frac{1}{\rho_n}\ln\left(\frac{|\xi|}{8\rho_n}\right)\right]d\xi \\ & + \int_{-\Delta\rho/2}^{\Delta\rho/2}\int_0^{\pi}\left\{\frac{\cos\phi' e^{-jkR_{nn}} - 1}{R_{nn}}\right\}d\phi'd\xi\Bigg\}. \end{aligned} \tag{45}$$

The unbounded part of the elliptic integral is added to and subtracted from the integrand of (42). The integral of the added term becomes the first term of (45) while the subtracted term remains in the integrand of the first integral of (45). Therefore, both integrals of (45) have very slowly varying integrands and can be integrated numerically with ease.

The integration indicated in (30c) can be performed analytically and, as a result, Y^c_{mn} becomes

$$Y^c_{mn} = -\frac{1}{\eta_c \ln\frac{b}{a}} \frac{1}{\rho_m} \ln\left(\frac{\rho_{n+\frac{1}{2}}}{\rho_{n-\frac{1}{2}}}\right)\left[\frac{1 - \Gamma e^{-j2k_c L}}{1 + \Gamma e^{-j2k_c L}}\right]$$

$$- \frac{k_c}{\eta_c} \sum_{q=1}^{\infty} \frac{1}{\chi_q N_q^2} \frac{d}{d\rho} \Phi_q(\rho_m)\left[\Phi_q(\rho_{n+\frac{1}{2}}) - \Phi_q(\rho_{n-\frac{1}{2}})\right] \quad (46)$$

in which $\rho_{n+\frac{1}{2}} = a + n\Delta\rho$ and $\rho_{n-\frac{1}{2}} = a + \Delta\rho(n-1)$ and in which $\frac{d}{d\rho}\Phi_q(\ _m)$ means $\left[\frac{d}{d\rho}\Phi_q(\rho)\right]_{\rho=\rho_m}$.

The series in Y^c_{mn} must be summed efficiently if the numerical procedure described here is to be practicable. This is particularly true in regard to Y^c_{mn} because of the need to solve a transcendental equation to determine the transverse eigenvalue k_{tq} of (6) prior to the computation of each series term. To this end Kummer's transformation [9] is used to accelerate convergence. To employ this technique, one determines the q^{th} term for large q of his series and then finds another series with known sum and the same large-index q^{th} term. Even though Kummer's transformation is applied to the series of the present problem under the condition that the guide is below cutoff of the higher-order modes, $k^2<k^2_{tq}$, which is the case of major practical interest, the procedure is immediately extendable to the cases in which higher-order modes do propagate.

One can show readily that

$$k_{tq} \xrightarrow[q\to\infty]{} \frac{q\pi}{b-a} \quad (47a)$$

and subsequently that

$$\frac{1}{\chi_q N_q^2}\frac{d}{d\rho}\,\Phi_q(\rho_m)\;\Phi_q(\rho_{n\pm\frac{1}{2}}) \xrightarrow[q\to\infty]{} C_{mn\pm\frac{1}{2}}\left\{\frac{\sin q\;\theta_{mn\pm\frac{1}{2}}}{q^2}-\frac{\sin q\;\Omega_{mn\pm\frac{1}{2}}}{q^2}\right\} \tag{47b}$$

where

$$C_{mn\pm\frac{1}{2}} = j\,\frac{1}{\pi^2}\,\frac{b-a}{\sqrt{\rho_m\;\rho_{n\pm\frac{1}{2}}}} = j\,\frac{1}{\pi^2}\,\frac{b-a}{\sqrt{(a+\Delta\rho[m-\frac{1}{2}])\,(a+\Delta\rho[(n-\frac{1}{2})\pm\frac{1}{2}])}}\;, \tag{48a}$$

$$\theta_{mn\pm\frac{1}{2}} = \frac{\pi}{b-a}\;(\rho_m+\rho_{n\pm\frac{1}{2}}-2a) = \frac{\pi\Delta\rho}{b-a}\;[(m+n-1)\pm\tfrac{1}{2}]\;, \tag{48b}$$

and

$$\Omega_{mn\pm\frac{1}{2}} = \frac{\pi}{b-a}\;(\rho_m-\rho_{n\pm\frac{1}{2}}) = \frac{\pi\Delta\rho}{b-a}\;[(m-n)\mp\tfrac{1}{2})]\;. \tag{48c}$$

In [10] the series below and its closed-form sum are listed:

$$\sum_{q=2}^{\infty} S_q(\alpha) = \delta(\alpha),\quad 0<\alpha<2\pi \tag{49a}$$

where

$$S_q(\alpha) = \frac{\sin q\alpha}{q^2-1} \tag{49b}$$

and

$$\delta(\alpha) = \left[\frac{1}{4}-\ln(2\sin\frac{\alpha}{2})\right]\sin\alpha,\quad 0<\alpha<2\pi\;. \tag{49c}$$

Notice that, apart from the factor $C_{mn\pm\frac{1}{2}}$, S_q exhibits the form of the right side of (47b) when $q\to\infty$. Applying Kummer's transformation to the series in Y^c_{mn}, one arrives at

$$Y^c_{mn} = -\frac{1}{\eta_c \ln\frac{b}{a}} \frac{1}{\rho_m} \ln\left(\frac{\rho_{n+\frac{1}{2}}}{\rho_{n-\frac{1}{2}}}\right)\left[\frac{1 - \Gamma\, e^{-j2k_cL}}{1 + \Gamma\, e^{-j2k_cL}}\right]$$

$$- \frac{k_c}{\eta_c \chi_1 N_1^2} \frac{d}{d\rho}\, \Phi_1(\rho_m)\left[\Phi_1(\rho_{n+\frac{1}{2}}) - \Phi_1(\rho_{n-\frac{1}{2}})\right]$$

$$- \frac{k_c}{\eta_c} \sum_{q=2}^{\infty} \left\{\frac{1}{\chi_q N_q^2} \frac{d}{d\rho}\, \Phi_q(\rho_m)\left[\Phi_q(\rho_{n+\frac{1}{2}}) - \Phi_q(\rho_{n-\frac{1}{2}})\right]\right.$$

$$- C_{mn+\frac{1}{2}}\left[S_q(\theta_{mn+\frac{1}{2}}) - S_q(\Omega_{mn+\frac{1}{2}})\right]$$

$$\left. + C_{mn-\frac{1}{2}}\left[S_q(\theta_{mn-\frac{1}{2}}) - S_q(\Omega_{mn-\frac{1}{2}})\right]\right\}$$

$$- \frac{k_c}{\eta_c} C_{mn+\frac{1}{2}}\left[\delta(\theta_{mn+\frac{1}{2}}) - \frac{\Omega_{mn+\frac{1}{2}}}{|\Omega_{mn+\frac{1}{2}}|}\delta(|\Omega_{mn+\frac{1}{2}}|)\right]$$

$$+ \frac{k_c}{\eta_c} C_{mn-\frac{1}{2}}\left[\delta(\theta_{mn-\frac{1}{2}}) - \frac{\Omega_{mn-\frac{1}{2}}}{|\Omega_{mn-\frac{1}{2}}|}\delta(|\Omega_{mn-\frac{1}{2}}|)\right] \qquad (50)$$

which converges in very few terms. Absolute values are used above because $\Omega_{mn+\frac{1}{2}}$ can be negative and, as indicated, (49c) is valid only for $0<\alpha<2\pi$. Since, for $\alpha<0$, $\sin\alpha = -\sin|\alpha|$, we can write

$$\sin\alpha = \frac{\alpha}{|\alpha|} \sin|\alpha| \qquad \text{for all } \alpha \ . \qquad (51)$$

This can be used to advantage to rewrite (49) as

$$\sum_{q=2}^{\infty} \frac{\sin q\,\alpha}{q^2-1} = \frac{\alpha}{|\alpha|} \sum_{q=2}^{\infty} \frac{\sin q\,|\alpha|}{q^2-1} = \frac{\alpha}{|\alpha|} \left[\frac{1}{4} - \ell n(2 \sin \frac{|\alpha|}{2})\right] \sin|\alpha|$$

$$\text{for } -2\pi<\alpha<2\pi \qquad (52a)$$

or

$$\sum_{q=2}^{\infty} S_q(\alpha) = \frac{\alpha}{|\alpha|} \left[\frac{1}{4} - \ell n(2 \sin \frac{|\alpha|}{2})\right] \sin\,|\alpha|, \quad -2\pi<\alpha<2\pi. \qquad (52b)$$

REFERENCES

1. Harrison, M.G., and C.M. Butler, "An analytical and experimental investigation of planar discontinuities in coaxial waveguides," Technical Report AFWL-TR-79-187, Air Force Weapons Laboratory, Kirtland Air Force Base, NM 87117; March, 1981.

2. Harrington, R. F., Time-Harmonic Electromagnetic Fields, McGraw-Hill Book Company, New York; 1961.

3. Harrington, R. F., Field Computations by Moment Methods, Macmillan, New York; 1968.

4. Butler, C. M., "Evaluation of potential integral at singularity of exact kernel in thin-wire calculations," IEEE Trans. on Antennas and Propagat., Vol. AP-23, No. 2, pp. 293-295; March, 1975.

5. Butler, C. M., and D. R. Wilton, "Analysis of various numerical techniques applied to thin-wire scatterers," IEEE Trans. on Antennas and Propagat., Vol. AP-23, No. 4, pp. 534-540; July, 1975.

6. Butler, C. M., D. R. Wilton, and A. W. Glisson, "Fundamentals of numerical solution methods in electromagnetics—short course notes," University of Mississippi, University, MS 38677; March, 1982.

7. Butler, C. M., and L. L. Tsai, "An alternate frill field formulation," IEEE Trans. on Antennas and Propagat., Vol. AP-21, No. 1, pp. 115-116; January, 1973.

8. Dwight, H. B., Tables of Integrals and Other Mathematical Data, Macmillan, New York; 1961.

9. Knopp, K., Theory and Application of Infinite Series (trans.), Hofner, New York; 1971.

10. Jolley, L. B. W., Summation of Series, Dover, New York; 1961.

3. FORMULATION OF INTEGRAL EQUATION FOR GROUND STAKE ANTENNA

The analysis of the behavior of the current and charge on a straight cylindrical antenna which resides in two contiguous half spaces is a major portion of this investigation. As a model for study of the behavior of charge and current everywhere—in particular, at the wire ends in lossy media and at the interface between the two half spaces—the current and charge on the structure shown in cross section in Fig. 1 is studied. This section is devoted to the formulation of the integral equation for the antenna structure of Fig. 1. In this figure, one sees a circular cylindrical (tubular) antenna, partially in one half space and partially in the other, which intersects perpendicularly the planar interface between the two media. In general the cylindrical antenna does not meet the thin-wire conditions and it is driven by the slice generator illustrated. Due to the symmetry of the structure and excitation, the current on the perfectly electrically conducting (PEC) antenna is z-directed and circumferentially independent.

An integral equation for the current on this antenna is formulated with care that it be amenable to numerical solution. The equation incorporates the exact kernel and special forms of the so-called Sommerfeld integrals. The initial phase of the formulation is the derivation of suitable Green's functions for the magnetic vector potential in the two-media space of Fig. 1 due to a ring dipole source. Then the integral equation—actually, coupled integral equations—is developed by enforcing the condition that the total electric field tangential to and evaluated on the PEC surface of the cylindrical tube be zero.

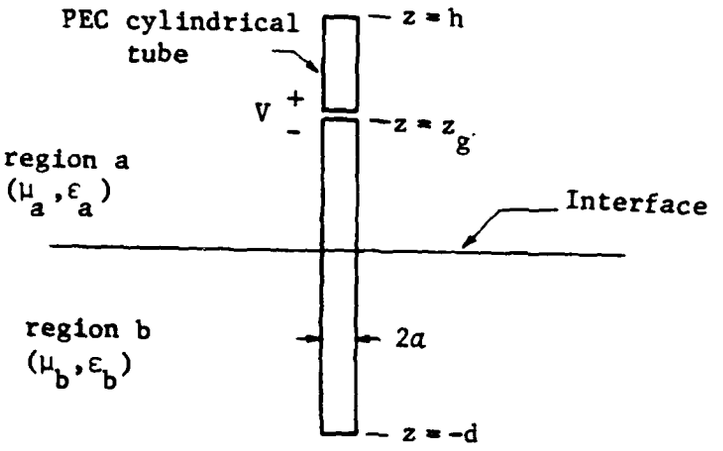

Fig. 1. Cross sectional view of antenna in two contiguous half spaces.

Green's Functions

In Fig. 2 is illustrated an ensemble of elementary dipoles all on a circle of radius ρ' in a plane, all in the same direction perpendicular to this plane, and each vanishingly close to its immediate neighbor. This so-called ring dipole is placed in a cylindrical coordinate system with the center of the ring on the z axis at $z = z'$ and with its plane parallel to the $z = 0$ coordinate plane. The elementary dipoles of the ensemble are z-directed. It should be clear that such a ring dipole source constitutes a volume current density $\underline{J}$ given by

$$\underline{J}(\underline{r}) = \hat{\underline{z}}\ \delta(\rho-\rho')\ \delta(z-z') \quad . \tag{1}$$

It should be equally clear that the magnetic vector potential due to $\underline{J}$ of (1), with $\rho' = a$ and with this current in the appropriately specified physical environment, is the Green's function for the vector potential due to the current on the cylinder of Fig. 1.

The Green's function needed in the integral equation for the cylindrical antenna is the magnetic vector potential due the ring dipole of Fig. 2 in the two-media space of Fig. 1. This vector potential must be known for z in the interval (-d,h) when the ring dipole is located in (0,h) and when it is located in (-d,0). To obtain the vector potential we determine the solution of the wave equation subject to the radiation condition with the ring dipole in (0,h) and then with it in (-d,0). We construct the solution as the sum of a homogeneous and a particular solution, and, in both cases, we take the particular solution to be the vector potential due to the ring dipole located in unbounded space, i.e., homogeneous space of infinite extent. Hence, in what follows immediately below, the wave

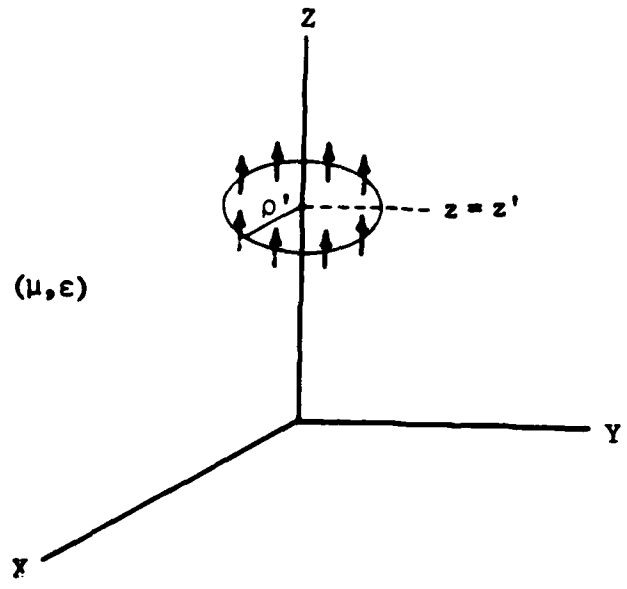

Fig. 2. Z-directed ring dipole in unbounded space.

equation is solved for the vector potential due to the ring dipole in unbounded space. Next, the appropriate wave equation is solved for the vector potential due to the ring dipole in region a and, then, the appropriate wave equation is solved for the vector potential due to the ring dipole in region b.

The Hankel transform (zero order) is well suited as an aid in solving the wave equation in cylindrical coordinates and, therefore, it is employed below. For a given function $f(\rho)$ the Hankel transform pair is

$$\tilde{f}(\lambda) = \int_0^\infty \rho f(\rho)\ J_0(\lambda\rho)d\rho \tag{2a}$$

$$f(\rho) = \int_0^\infty \lambda\tilde{f}(\lambda)\ J_0(\lambda\rho)d\lambda \tag{2b}$$

where $\tilde{f}(\lambda)$ is the Hankel transform of $f(\rho)$.

Green's Function for Ring Dipole in Unbounded Space. For the ring dipole located in unbounded space characterized by (μ,ε) (Fig. 2), the vector potential $\underline{A} = A_z(\rho,z)\hat{\underline{z}}$ has the single component A_z which satisfies

$$(\nabla^2_{\rho z} + k^2)\ A_z(\rho,z) = -\mu\delta(\rho-\rho')\ \delta(z-z') \tag{3a}$$

or

$$\frac{1}{\rho}\frac{\partial}{\partial\rho}(\rho A_z) + \frac{\partial^2}{\partial z^2}A_z + k^2A_z = -\mu\delta(\rho-\rho')\ \delta(z-z') \tag{3b}$$

where $k^2 = \omega^2\mu\varepsilon$, and the field computed from A_z must satisfy the usual radiation condition. Taking the Hankel trarsform of the two

sides of (3b) (or, equivalently, multiplying both sides by $\rho J_0(\lambda\rho)$ and integrating over $(0,\infty)$) yields

$$\int_0^\infty \rho \left\{\frac{1}{\rho}\frac{\partial}{\partial\rho}\left(\rho A_z(\rho,z)\right)\right\} J_0(\lambda\rho)d\rho + \left(\frac{\partial^2}{\partial z^2} + k^2\right)\int_0^\infty \rho A_z(\rho,z)\, J_0(\lambda\rho)d\rho$$

$$= -\mu\rho' J_0(\lambda\rho')\, \delta(z-z') \ . \tag{4}$$

In view of the properties that A_z must exhibit for $\rho \to 0$ and $\rho \to \infty$, one can show by integration by parts twice that

$$\int_0^\infty \rho \left\{\frac{1}{\rho}\frac{\partial}{\partial\rho}\left(\rho A_z(\rho,z)\right)\right\} J_0(\lambda\rho)d\rho = -\lambda^2\int_0^\infty \rho\, A_z(\rho,z)\, J_0(\lambda\rho)d\rho \tag{5}$$

whose right hand side is recognized to be the Hankel transform $\tilde{A}_z(\lambda,z)$ of $A_z(\rho,z)$. Substitution of (5) into (4) leads to the differential equation

$$\left(\frac{d^2}{dz^2} + \beta^2\right)\tilde{A}_z(\lambda,z) = -\mu\rho'\, J_0(\lambda\rho')\, \delta(z-z') \tag{6a}$$

where

$$\beta^2 = k^2 - \lambda^2 \ . \tag{6b}$$

The solution of this differential equation is

$$\tilde{A}_z(\lambda,z) = -j\frac{\mu}{2}\,\rho' J_0(\lambda\rho')\,\frac{e^{-j\beta|z-z'|}}{\beta} \tag{7}$$

from which A_z is found as the inverse Hankel transform of $\tilde{A}_z$ to be

$$A_z(\rho,z) = -j\frac{\mu}{2}\,\rho' \int_0^\infty \lambda\, J_0(\lambda\rho')\,\frac{e^{-j\beta|z-z'|}}{\beta}\, J_0(\lambda\rho)d\lambda \ . \tag{8}$$

The form of the solution (7) of the differential equation (6a) adopted for $\tilde{A}_z$ is such that a root β of (6b) can be selected in such a way that $A_z(\rho,z)$ of (8) represents a wave traveling away from the ring dipole and, in particular, satisfies the radiation condition as $|z| \to \infty$. The proper branch of β may be defined by means of

$$\mathrm{Im}(\beta) < 0 \ . \tag{9}$$

Branch cuts which are consistent with (9) and which restrict λ to the proper sheet in the λ-plane are illustrated in Fig. 3. Also illustrated in Fig. 3 is the integration path of the integral of (8). One notes that for k real the path must be deformed into the first quadrant to avoid the singular point of β at $\lambda = k$, while in the lossy-medium case for which k is complex the singular point is not on the integration path and deformation is unnecessary. The condition (9) endows the integral (8) with properties which allow one to deform the integration contour off the positive real axis of the λ-plane. If k is real and deformation of the path of the integral from the real line is not to be employed, β may be defined in the simple way below:

$$\beta = \begin{cases} \sqrt{k^2 - \lambda^2} \ , & k^2 > \lambda^2 \\ -j\sqrt{\lambda^2 - k^2} \ , & k^2 < \lambda^2 \ . \end{cases} \tag{10}$$

For some applications, it is convenient to convert (8) to an integral over $(-\infty,\infty)$. To do this, one replaces one of the Bessel functions of (8) by its equivalent [1] in terms of Hankel functions,

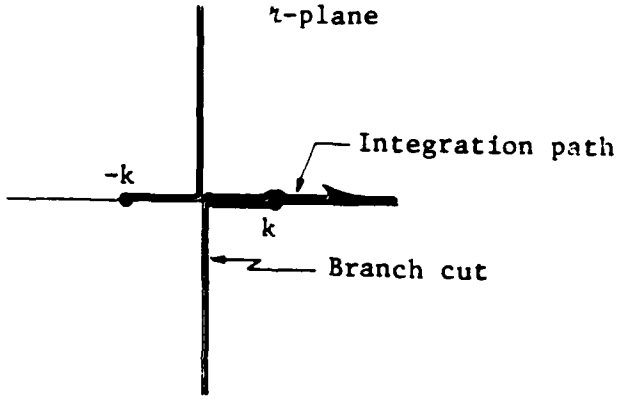

(a)

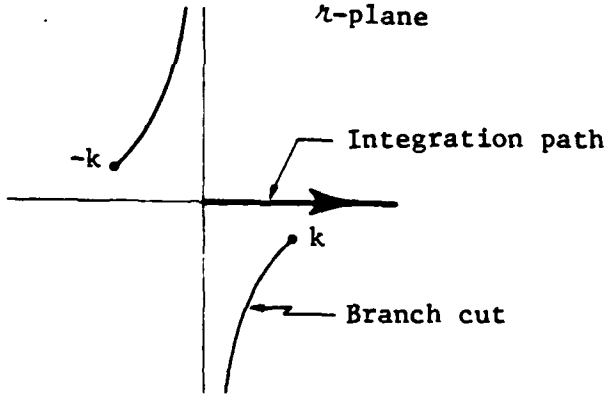

(b)

Fig. 3. Branch points ($\lambda = \pm k$), branch cuts, and integration path for (8) in the λ-plane (a) lossless case, (b) lossy case.

$$J_0(\zeta) = \frac{1}{2}\,[H_0^{(2)}(\zeta) - H_0^{(2)}(\zeta e^{-j\pi})], \tag{11}$$

replaces the integration variable by its negative in one of the integrals, makes use of $J_0(-\zeta) = J_0(\zeta)$, and combines the two integrals to obtain

$$A_z(\rho,z) = \begin{cases} -j\,\frac{\mu}{4}\,\rho' \int_{-\infty}^{\infty} \lambda J_0(\lambda\rho')\,\frac{e^{-j\beta|z-z'|}}{\beta}\,H_0^{(2)}(\lambda\rho)\,d\lambda \quad , \rho>\rho' & (12a) \\ -j\,\frac{\mu}{4}\,\rho' \int_{-\infty}^{\infty} \lambda\, H_0^{(2)}(\lambda\rho')\,\frac{e^{-j\beta|z-z'|}}{\beta}\,J_0(\lambda\rho)\,d\lambda \quad , \rho<\rho'. & (12b) \end{cases}$$

The path of integration of the integrals of (12) and the branch cuts of β and $H_0^{(2)}$ are illustrated in Fig. 4.

Green's Function for Ring Dipole in Region A. In this subsection, we determine the magnetic vector potential due to a ring dipole in one homogeneous half space which is in contact with a second homogeneous half space of different electromagnetic properties. The two half spaces are separated by a planar interface and the ring dipole of radius ρ' is above and perpendicular to this plane as illustrated in Fig. 5, where one observes that the ring dipole is on the z coordinate axis at $z = z'$. The upper half space is designated region a and the lower half space is designated region b; quantities peculiar to region a carry subscript or superscript "a" while those peculiar to region b carry "b." In the z direction,

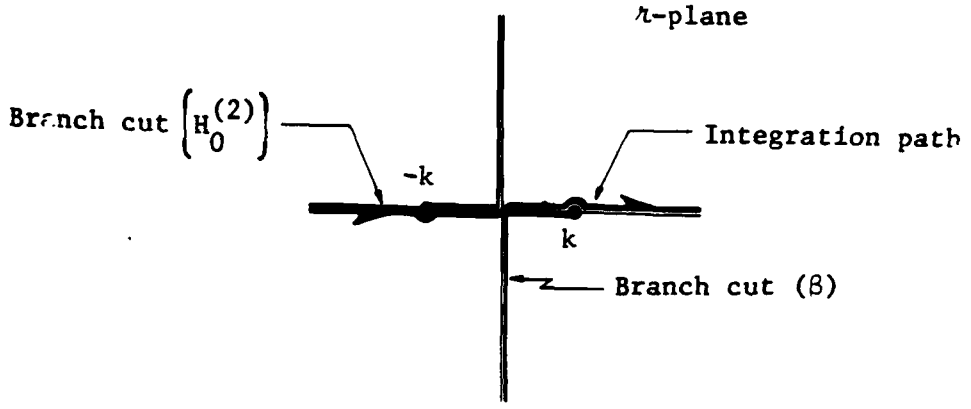

(a)

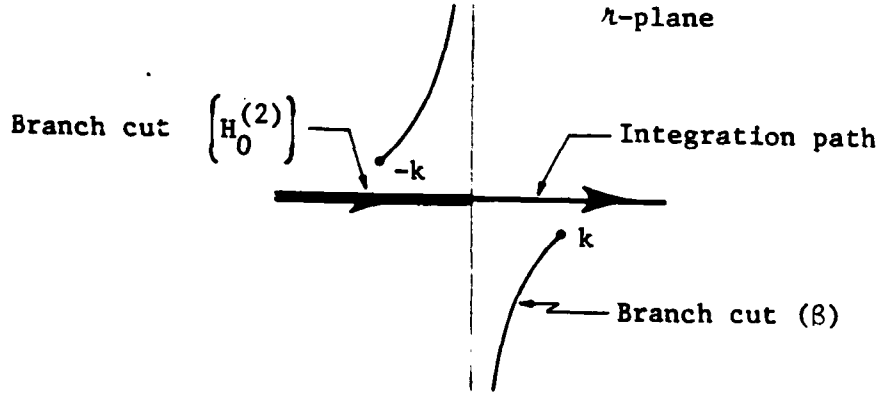

(b)

Fig. 4. Branch points and cuts of β and $H_0^{(2)}$, and integration path for (12) in λ-plane: (a) lossless case, (b) lossy case.

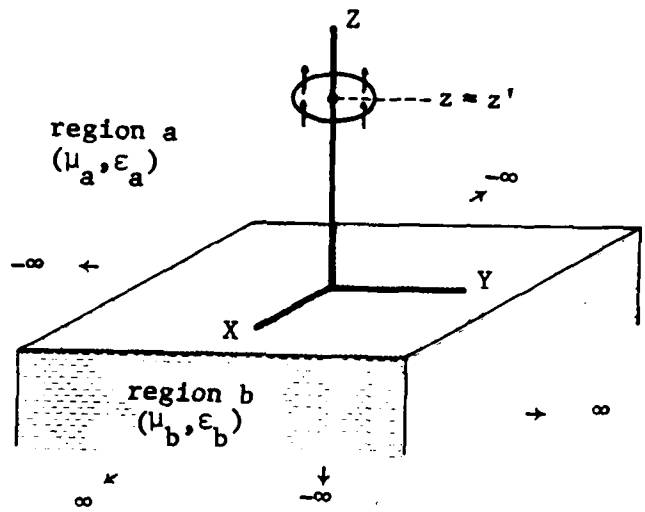

Fig. 5. Ring dipole on z axis in infinite half space (region a) radiating in the presence of contiguous infinite half space (region b).

region a extends from 0 to ∞ and region b extends from 0 to $-\infty$, while both regions extend from $-\infty$ to ∞ in the x and y directions.

The vector potential due to the ring dipole is ϕ-independent and it must satisfy the wave equation in each region. In region a the vector potential designated $A_z^a(\rho,z)$ satisfies

$$(\nabla_{\rho z}^2 + k_a^2)\, A_z^a(\rho,z) = -\mu_a\, \delta(\rho-\rho')\, \delta(z-z'), \quad z>0,\ z'>0 \tag{13}$$

while that in region b designated $A_z^b(\rho,z)$ satisfies

$$(\nabla_{\rho z}^2 + k_b^2)\, A_z^b(\rho,z) = 0\ ,\ z<0\ \ ,\ \ z'>0 \tag{14}$$

From knowledge of A_z^a and A_z^b the field components in the two regions can be determined in the usual way according to

$$E_\rho^{\substack{a\\b}} = -j\,\frac{\omega}{k_{\substack{a\\b}}^2}\,\frac{\partial^2}{\partial\rho\partial z}\,A_z^{\substack{a\\b}}\ , \tag{15a}$$

$$E_z^{\substack{a\\b}} = -j\,\frac{\omega}{k_{\substack{a\\b}}^2}\left(k_{\substack{a\\b}}^2 + \frac{\partial^2}{\partial z^2}\right)A_z^{\substack{a\\b}}\ , \tag{15b}$$

and

$$H_\phi^{\substack{a\\b}} = -\frac{1}{\mu_{\substack{a\\b}}}\,\frac{\partial}{\partial\rho}\,A_z^{\substack{a\\b}}\ . \tag{16}$$

We observe that Eq. (14) is a homogeneous differential equation since no source exists in region b while the right hand side of Eq. (13) accounts for the presence of the ring dipole of radius ρ' at $z=z'$. The

field computed from A_z^a and A_z^b must safisfy the radiation condition and the components which are parallel to the interface must be continuous at $z = 0$. These continuity requirements can be stated as

$$\frac{1}{k_a^2} \frac{\partial^2}{\partial\rho\partial z} A_z^a = \frac{1}{k_b^2} \frac{\partial^2}{\partial\rho\partial z} A_z^b \ , \text{ at } z = 0 \tag{17a}$$

and

$$\frac{1}{\mu_a} \frac{\partial}{\partial\rho} A_z^a = \frac{1}{\mu_b} \frac{\partial}{\partial\rho} A_z^b \ , \text{ at } z = 0 \ . \tag{17b}$$

Eqs.(13) and (14), the radiation condition, and the continuity requirements (17) completely characterize the vector potential in the two regions due to the ring dipole.

We employ the Hankel transform to solve (13) and (14) subject to (15) and the radiation condition. Transforming both sides of (13) and (14) yields, respectively,

$$\left(\frac{d^2}{dz^2} + \beta_a^2\right) \tilde{A}_z^a(\lambda,z) = -\mu_a \rho' \, J_0(\lambda\rho') \, \delta(z-z'), \ z>0, \ z'>0 \tag{18}$$

and

$$\left(\frac{d^2}{dz^2} + \beta_b^2\right) \tilde{A}_z^b(\lambda,z) = 0, \ z<0, \ z'>0 \tag{19}$$

where $\tilde{A}_z^a$ and $\tilde{A}_z^b$ are the Hankel transforms of A_z^a and A_z^b and where

$$\beta_{a\atop b}^2 = k_{a\atop b}^2 - \lambda^2 \ . \tag{20}$$

The solution of the differential equation (18) is obviously

$$\tilde{A}_z^a = -j \frac{\mu_a}{2} \rho' J_0(\lambda\rho') \frac{e^{-j\beta_a|z-z'|}}{\beta_a}$$

$$-j \frac{\mu_a}{2} \rho' J_0(\lambda\rho') \, C(\lambda) \frac{e^{-j\beta_a z}}{\beta_a} \qquad (21)$$

where the first term is the particular solution and the second is the homogeneous solution. $C(\lambda)$ is an unknown function of λ to be determined subsequently. In general, the homogeneous solution contains a term proportional to $e^{+j\beta_a z}$ but, if such were added to (21), it would lead to a term in A_z^a which would be physically unacceptable in that it would represent a wave propagating in the negative z direction for $z>z'$. Observe, too, that the particular solution is the same as (7) with μ and β replaced μ_a and β_a. A_z^a is now obtained by taking the inverse Hankel transform of (21):

$$A_z^a(\rho,z) = -j \frac{\mu_a}{2} \rho' \int_0^\infty \lambda \, J_0(\lambda\rho') \frac{e^{-j\beta_a|z-z'|}}{\beta_a} J_0(\lambda\rho) d\lambda$$

$$-j \frac{\mu_a}{2} \rho' \int_0^\infty \lambda \, J_0(\lambda\rho') \, C(\lambda) \frac{e^{-j\beta_a z}}{\beta_a} J_0(\lambda\rho) d\lambda \, , \quad \begin{matrix} z>0, \\ z'>0 \end{matrix} . \qquad (22)$$

The first term of (22) is the vector potential due to the ring dipole in medium (μ_a,ε_a), determined as if the medium were of infinite extent, while the second term is the vector potential of the field resulting from scattering of the ring dipole field by the interface at $z = 0$.

Turning to the differential equation (19), we write its solution as

$$\tilde{A}_z^b(\lambda,z) = -j\frac{\mu_b}{2}\rho' J_0(\lambda\rho')\, B(\lambda)\frac{e^{j\beta_b z}}{\beta_a}, \quad z<0,\ z'>0 \tag{23}$$

which is clearly a special form of the homogeneous solution of this equation having no term proportional to $e^{-j\beta_b z}$. The form of (23) ensures that the final solution in region b represent a wave traveling away from the interface. Thus, A_z^b is found from the inverse Hankel transform to be

$$A_z^b(\rho,z) = -j\frac{\mu_b}{2}\rho' \int_0^\infty \lambda\, J_0(\lambda\rho')\, B(\lambda)\frac{e^{j\beta_b z}}{\beta_a} J_0(\lambda\rho)d\lambda\,, \quad z<0,\ z'>0\ . \tag{24}$$

To enforce (17b), one requires

$$B(\lambda) = C(\lambda) + e^{-j\beta_a z'}, \quad z'>0 \tag{25}$$

which, together with (24), yields

$$A_z^b(\rho,z) = -j\frac{\mu_b}{2}\rho' \int_0^\infty \lambda\, J_0(\lambda\rho')\left[C(\lambda) + e^{-j\beta_a z'}\right]\frac{e^{j\beta_b z}}{\beta_a} J_0(\lambda\rho)d\lambda\ . \tag{26}$$

If, in addition, (17a) is enforced, one finds that

$$\beta_a\left(e^{-j\beta_a z'} - C(\lambda)\right) = \beta_b\left(e^{-j\beta_a z'} + C(\lambda)\right) \tag{27}$$

must be satisfied from which $C(\lambda)$ is determined to be

$$C(\lambda) = \Gamma\, e^{-j\beta_a z'} \tag{28a}$$

where

$$\Gamma = \frac{\frac{\beta_a}{\varepsilon_a} - \frac{\beta_b}{\varepsilon_b}}{\frac{\beta_a}{\varepsilon_a} + \frac{\beta_b}{\varepsilon_b}} \quad . \tag{28b}$$

Finally, with $C(\lambda)$ of (28) in (22) and (26), one arrives at the desired vector potentials in the two regions:

$$A_z^a(\rho,z) = -j\frac{\mu_a}{2}\rho' \int_0^\infty \lambda\, J_0(\lambda\rho')\, \frac{e^{-j\beta_a|z-z'|}}{\beta_a} J_0(\lambda\rho)d\lambda$$

$$-j\frac{\mu_a}{2}\rho' \int_0^\infty \lambda\, J_0(\lambda\rho')\Gamma\, \frac{e^{-j\beta_a(z+z')}}{\beta_a} J_0(\lambda\rho)d\lambda \ ,$$

$$z>0,\ z'>0 \tag{29a}$$

and

$$A_z^b(\rho,z) = -j\frac{\mu_b}{2}\rho' \int_0^\infty \lambda\, J_0(\lambda\rho')[1+\Gamma]\, \frac{e^{-j\beta_a z'}}{\beta_a} e^{j\beta_b z} J_0(\lambda\rho)d\lambda \ ,$$

$$z<0,\ z'>0 \ . \tag{29b}$$

The branch points and branch cuts for β_a and β_b, under the conditions that region a is lossless and region b is lossy, are illustrated in Fig. 6 where also is shown the path of integration for the integrals of (29).

By appealing to (11) and the procedure leading to (12), one can obtain the alternate forms for (29) that appear below. The path of integration for the integrals of (30) and (31) is illustrated in Fig. 7.

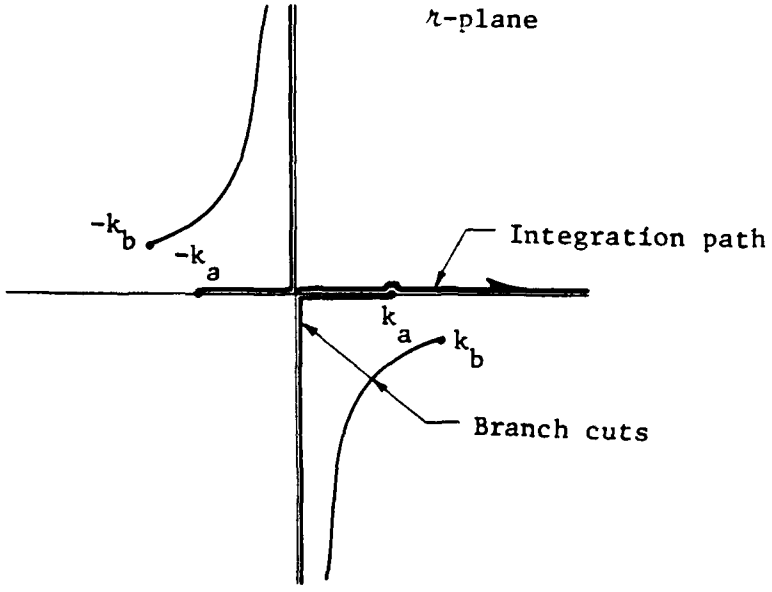

Fig. 6. Branch points and branch cuts for β_a and β_b and integration path for (29) and (33) in λ-plane: region a lossless, region b lossy.

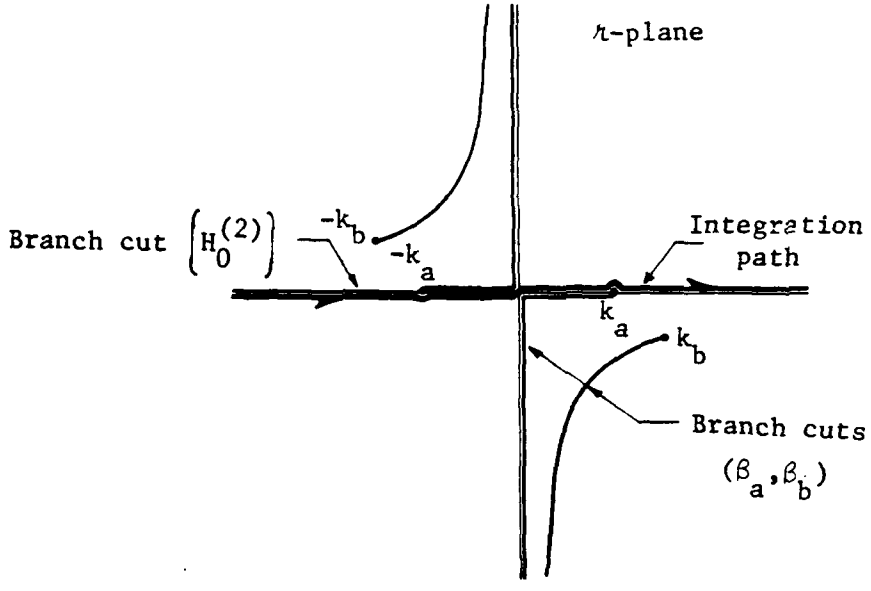

Fig. 7. Branch points and branch cuts for β_a, β_b, and $H_0^{(2)}$ and integration path for (30), (31), (34), and (35) in λ-plane: region a lossless, region b lossy.

$$A_z^a(\rho,z) = \begin{cases} -j\frac{\mu_a}{4}\rho'\int_{-\infty}^{\infty} \eta J_0(\eta\rho')\frac{e^{-j\beta_a|z-z'}}{\beta_a}H_0^{(2)}(\eta\rho)d\eta - j\frac{\mu_a}{4}\rho'\int_{-\infty}^{\infty} \eta J_0(\eta\rho')\Gamma\frac{e^{-j\beta_a(z+z')}}{\beta_a}H_0^{(2)}(\eta\rho)d\eta, \\ \qquad \rho>\rho',\ z>0,\ z'>0 \qquad (30a) \\ -j\frac{\mu_a}{4}\rho'\int_{-\infty}^{\infty} \eta H_0^{(2)}(\eta\rho')\frac{e^{-j\beta_a|z-z'|}}{\beta_a}J_0(\eta\rho)d\eta - j\frac{\mu_a}{4}\rho'\int_{-\infty}^{\infty} \eta H_0^{(2)}(\eta\rho')\Gamma\frac{e^{-j\beta_a(z+z')}}{\beta_a}J_0(\eta\rho)d\eta, \\ \qquad \rho<\rho',\ z>0,\ z'>0 \qquad (30b) \end{cases}$$

$$A_z^b(\rho,z) = \begin{cases} -j\frac{\mu_b}{4}\rho'\int_{-\infty}^{\infty} \eta J_0(\eta\rho')[1+\Gamma]\frac{e^{-j\beta_a z'}}{\beta_a}e^{j\beta_b z}H_0^{(2)}(\eta\rho)d\eta, \quad \rho>\rho',\ z<0,\ z'>0 \qquad (31a) \\ -j\frac{\mu_b}{4}\rho'\int_{-\infty}^{\infty} \eta H_0^{(2)}(\eta\rho')[1+\Gamma]\frac{e^{-j\beta_a z'}}{\beta_a}e^{j\beta_b z}J_0(\eta\rho)d\eta, \quad \rho<\rho',\ z<0,\ z'>0 \qquad (31b) \end{cases}$$

Green's Function for Ring Dipole in Region B

When the ring dipole of radius ρ' is located at $z = z'$ ($z'<0$) on the z axis in region b, the resulting vector potentials in the two regions satisfy

$$(\nabla^2_{\rho z} + k_a^2)\, A_z^a(\rho,z) = 0 \ , \ z>0, \ z'<0 \tag{32a}$$

and

$$(\nabla^2_{\rho z} + k_b^2)\, A_z^b(\rho,z) = -\mu_b\, \delta(\rho-\rho')\, \delta(z-z'), \ z<0, \ z'<0 \tag{32b}$$

plus, of course, the radiation condition. Also A_z^a and A_z^b must satisfy the continuity conditions (17). One may solve (32) subject to the stated conditions by a procedure paralleling that applied to (13) and (14). This procedure is not repeated here but the resulting solutions are recorded below:

$$A_z^a(\rho,z) = -j\,\frac{\mu_a}{2}\,\rho'\int_0^\infty \lambda\, J_0(\lambda\rho')[1-\Gamma]\,\frac{e^{j\beta_b z'}}{\beta_b}\, e^{-j\beta_a z}\, J_0(\lambda\rho)d\lambda \ ,$$

$$z>0, \ z'<0 \tag{33a}$$

and

$$A_z^b(\rho,z) = -j\,\frac{\mu_b}{2}\,\rho'\int_0^\infty \lambda\, J_0(\lambda\rho')\,\frac{e^{-j\beta_b|z-z'|}}{\beta_b}\, J_0(\lambda\rho)d\lambda$$

$$+j\,\frac{\mu_b}{2}\,\rho'\int_0^\infty \lambda\, J_0(\lambda\rho')\Gamma\,\frac{e^{j\beta_b(z+z')}}{\beta_b}\, J_0(\lambda\rho)d\lambda \ ,$$

$$z<0, \ z'<0 \ . \tag{33b}$$

The path of integration of the above integrals is the same as that illustrated in Fig. 6 for the integrals of (29). Alternate forms of

A_z^a and A_z^b are given on the next page. The path of integration for the integrals of (34) and (35) is illustrated in Fig. 7.

$$A_z^a(\rho,z) = \begin{cases} -j\frac{\mu_a}{4}\rho'\int_{-\infty}^{\infty} \eta\, J_0(\eta\rho')[1-\Gamma]\,\frac{e^{j\beta_b z'}}{\beta_b}\,e^{-j\beta_b z}\,H_0^{(2)}(\eta\rho)d\eta\,, \quad \rho>\rho',\ z>0,\ z'<0 & (34a) \\ -j\frac{\mu_a}{4}\rho'\int_{-\infty}^{\infty} \eta\, H_0^{(2)}(\eta\rho')[1-\Gamma]\,\frac{e^{j\beta_b z'}}{\beta_b}\,e^{-j\beta_a z}\,J_0(\eta\rho)d\eta\,, \quad \rho<\rho',\ z>0,\ z'<0 & (34b) \end{cases}$$

$$A_z^b(\rho,z) = \begin{cases} -j\frac{\mu_b}{4}\rho'\int_{-\infty}^{\infty} \eta\, J_0(\eta\rho')\,\frac{e^{-j\beta_b|z-z'|}}{\beta_b}\,H_0^{(2)}(\eta\rho)d\eta + j\frac{\mu_b}{4}\rho'\int_{-\infty}^{\infty} \eta\, J_0(\eta\rho')\Gamma\,\frac{e^{j\beta_b(z+z')}}{\beta_b}\,H_0^{(2)}(\eta\rho)d\eta\,, \\ \qquad \rho>\rho',\ z<0,\ z'<0 & (35a) \\ -j\frac{\mu_b}{4}\rho'\int_{-\infty}^{\infty} \eta\, H_0^{(2)}(\eta\rho')\,\frac{e^{-j\beta_b|z-z'|}}{\beta_b}\,J_0(\eta\rho)d\eta + j\frac{\mu_b}{4}\rho'\int_{-\infty}^{\infty} \eta\, H_0^{(2)}(\eta\rho')\Gamma\,\frac{e^{j\beta_b(z+z')}}{\beta_b}\,J_0(\eta\rho)d\eta\,, \\ \qquad \rho<\rho',\ z<0,\ z'<0 & (35b) \end{cases}$$

Integral Equations

The desired integral equations for the current on the ground-stake antenna of Fig. 1 now can be constructed. Due to the symmetry of the structure and the excitation, all quantities are independent of ϕ, and, also, the surface current $\underline{J}_s$ induced on the PEC cylindrical tube is entirely z-directed ($\underline{J}_s = J_z(z)\ \hat{\underline{z}}$). Under these conditions, the induced current produces an electric field whose ϕ component is zero so the only component of electric field produced by J_z which is tangential to the cylindrical surface of the antenna is the z component. For convenience, we define the total axial currents $I_a(z)$ and $I_b(z)$ on the portion of the cylinder in region a and region b, respectively, as

$$2\pi a J_z(z) = \begin{cases} I_a(z) & , \quad z \in (0,h) \\ I_b(z) & , \quad z \in (-d,0) \end{cases} \tag{36}$$

where, of course, a is the cylinder radius. Furthermore, we define E_z^{aa} and E_z^{ab} to be the tangential components of electric field induced on and evaluate at $\rho = a$ on the surface of the cylinder in region a, i.e., $z \in (0,h)$, due, respectively, to I_a and I_b, while E_z^{ba} and E_z^{bb} are defined to be the z components of electric field on the cylinder at $\rho = a$ in region b, i.e., $z \in (-d,0)$, again due, respectively, to I_a and I_b. Subject to these definitions, one can express the boundary condition that the total electric field tangential to and on the PEC cylindrical surface be zero by the following equations:

$$E_z^{aa}[I_a;z] + E_z^{ab}[I_b;z] = -V\ \delta(z-z_g), \quad z \in (0,h) \tag{37a}$$

$$E_z^{ba}[I_a;z] + E_z^{bb}[I_b;z] = 0 \quad , \quad z \in (-d,0) \quad , \tag{37b}$$

where $V\delta(z-z_g)$ accounts for the delta-gap source of strength V at $z = z_g$. By employing the vector potential Green's functions derived above, one can write (37) as

$$-j\frac{\eta_a}{4\pi k_a}\left(\frac{d^2}{dz^2} + k_a^2\right)\left[\int_0^h I_a(z')\ G^{aa}(z,z')dz' + \int_{-d}^0 I_b(z')\ G^{ab}(z,z')dz'\right]$$

$$= -V\delta(z-z_g), \quad z \in (0,h) \tag{38a}$$

and

$$-j\frac{\eta_b}{4\pi k_b}\left(\frac{d^2}{dz^2} + k_b^2\right)\left[\int_0^h I_a(z')\ G^{ba}(z,z')dz' + \int_{-d}^0 I_b(z')\ G^{bb}(z,z')dz'\right] = 0,$$

$$z \in (-d,0) \tag{38b}$$

where

$$G^{aa}(z,z') = K_a(z-z') - j\int_0^\infty \rho[J_0(\rho a)]^2\ \Gamma\frac{e^{-j\beta_a(z+z')}}{\beta_a}\,d\rho \tag{39a}$$

$$G^{ab}(z,z') = -j\int_0^\infty \rho[J_0(\rho a)]^2[1-\Gamma]\frac{e^{j\beta_b z'}}{\beta_b}e^{-j\beta_a z}\,d\rho \tag{39b}$$

$$G^{ba}(z,z') = -j\int_0^\infty \rho[J_0(\rho a)]^2[1+\Gamma]\frac{e^{-j\beta_a z'}}{\beta_a}e^{j\beta_b z}\,d\rho \tag{39c}$$

$$G^{bb}(z,z') = K_b(z-z') + j\int_0^\infty \gamma[J_0(\gamma a)]^2\Gamma\,\frac{e^{j\beta_b(z+z')}}{\beta_b}\,d\gamma \qquad (39d)$$

in which

$$K_p(z-z') = \frac{1}{2\pi}\int_{-\pi}^{\pi}\frac{e^{-jk_pR}}{R}\,d\phi' \quad , \quad p = a \text{ or } b, \qquad (40a)$$

with

$$R^2 = (z-z')^2 + 4a^2\sin^2\frac{\phi'}{2} \quad . \qquad (40b)$$

Fundamentally, the left hand sides of (38a) and (38b) are special cases of (15b) with appropriate Green's functions used in the vector potentials. G^{aa} and G^{ba} are (29a) and (29b), respectively, specialized to the present structure while G^{ab} and G^{bb} are specializations of (33a) and (33b), respectively. The first term in each of (29a) and (33b) is the vector potential due to the ring dipole in unbounded space. K_a in (39a) and K_b in (39d) account for the first terms, respectively, of (29a) and (33b). K_a and K_b of (40) are employed here in (39a) and (39d), rather than equivalent terms derived from the first terms of (29a) and (33b), simply because K_a and K_b are exact kernels of cylindrical antenna theory and computation involving such kernels has become routine. Of course, the integrals over $(0,\infty)$ of (39) could be replaced by integrals over $(-\infty,\infty)$ by appealing to (30), (31), (34), and (35). Such a replacement would allow one to convert integrals over the real line from $-\infty$ to ∞ to branch-cut integrals which in some cases are very attractive from a numerical computational point of view.

REFERENCE

1. Watson, G. N., Theory of Bessel Functions (2nd edition), Cambridge University Press, Cambridge; 1944.

4. COLLECTION OF EXPERIMENTAL DATA

In this section is found a description of the apparatus and procedures to be used to obtain data which will support the theoretical analysis of the foregoing sections. The experimental portion of this project involves two related efforts:

(1) measurement of the driving point impedance of wire antennas operated near an air/water interface; and

(2) determination of the electrical properties of the water.

Monopole antennas in various configurations are to be positioned at various heights above an air/water interface. The antenna driving point is to be below the water surface in some experiments and is to be above the water surface, but behind a conducting screen oriented normal to the water surface, in other experiments. During each experiment, samples of the water are to be gathered and each sample is to be subjected to several measurement procedures designed to determine the electrical properties of the water. The test antenna configurations and the techniques for determining water properties are described in detail later in this report.

The experimental effort has been organized into three phases:

PHASE I - Design and construction of apparatus
PHASE II - Experiments involving antenna driving point below water surface
PHASE III - Experiments involving antenna driving points above water surface, but behind a conducting screen.

PHASE I - Design and Construction of Apparatus

Water Tank. Design and construction of a suitable water tank represents the most difficult and expensive task of this phase. Electromagnetic considerations dictated that the tank should be of non-metallic

construction, should provide a water surface range of approximately 2.5 m (or 5λ in air at 600 Mhz), and should provide a water depth of approximately 1.1 m (or 20λ in water at 600 Mhz). When these considerations were balanced against available space and materials and the fabrication capabilities of this organization, a general specification was made for a wooden tank 16 ft by 16 ft by 4 ft - 4 in, overall. Such a tank would provide a water surface 4.67 m (15 ft - 4 in) by 4.67 m and a water depth of 1.22 m (4 ft). (See Fig. 1)

Before proceeding with tank construction, it was necessary to verify adequate floor strength and drainage capacity and to modify the building to provide a high-capacity water supply (2-in line, 90 psi) and to accomodate suspension of panels of anechoic materials above and around the water tank. This was done by University of Mississippi Physical Plant personnel at the expense of the School of Engineering.

Details of tank construction can be seen in Figs. 1 and 2. An underlying consideration in the design of the tank was that it be capable of disassembly for economical storage. Accordingly, the floor was constructed in four 8 ft by 8 ft sections and each wall was constructed as a separate section. The framework for floor and walls is of 2 x 4 pine on 16-in centers with bracing at 16-in intervals. The decking (3/4-in plywood) and the wall panels (1/2-in plywood) were nailed and glued to the framework. The floor sections were bolted to the floor and to adjacent wall sections, using 1/2-in cap screws with 2-in fender washers at 16-in intervals. Buttresses were added at the centerline of each wall section to reduce bowing.

In the original design, the tank was to be made watertight by caulking the seams between pre-fabricated sections with silicon rubber

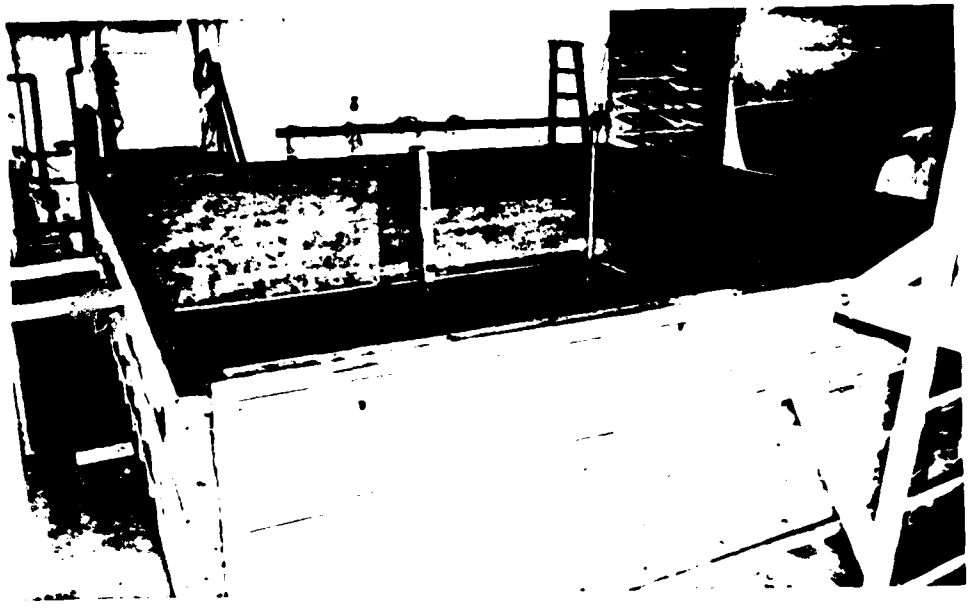

(a)

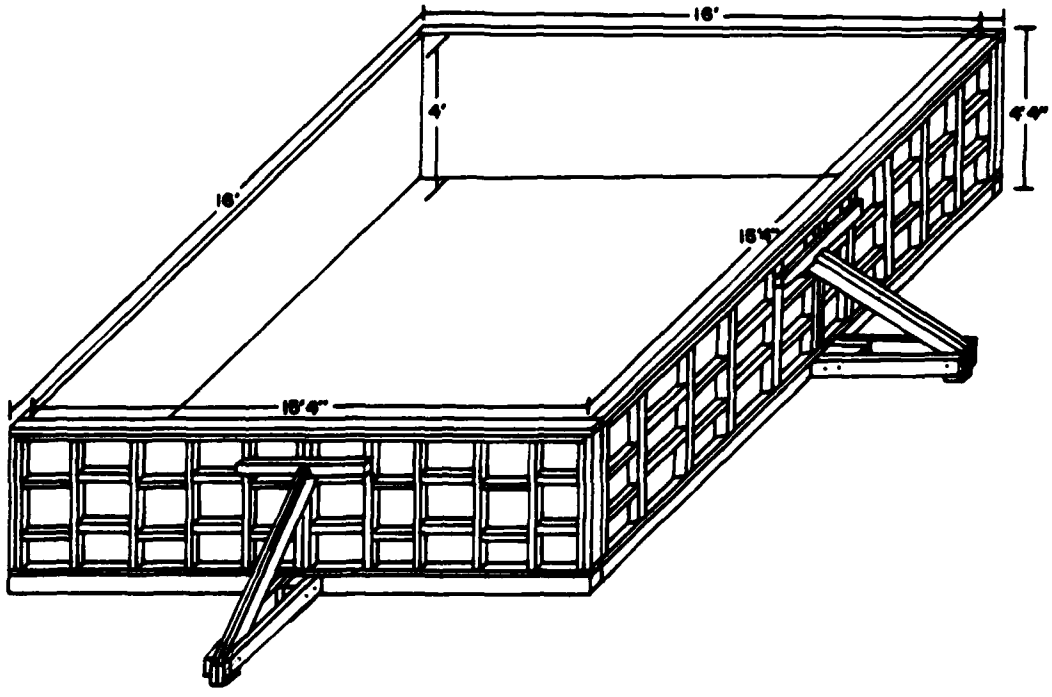

(b)

Fig. 1. Water tank.

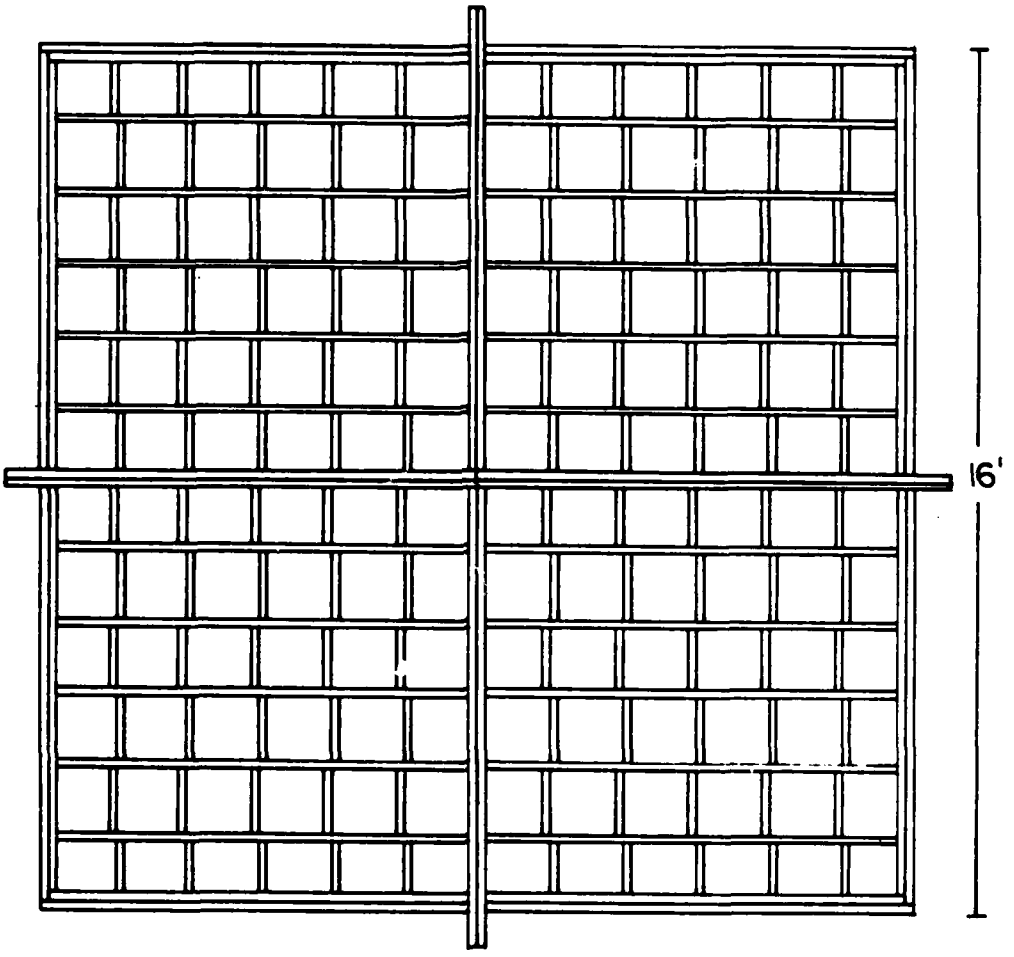

(a)

Fig. 2. Construction of floor frame for water tank.

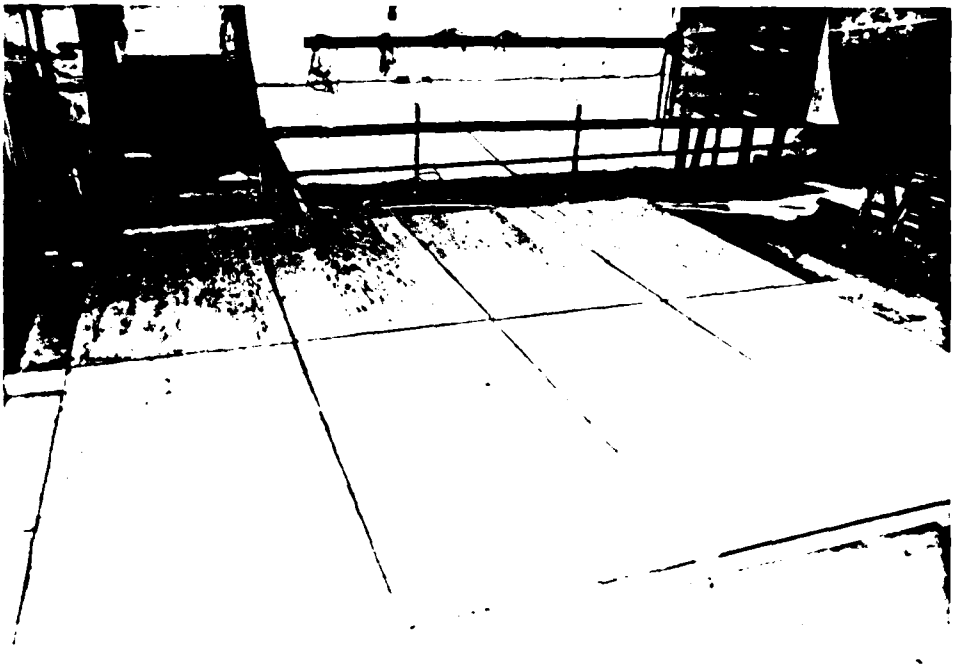

Fig. 2b.

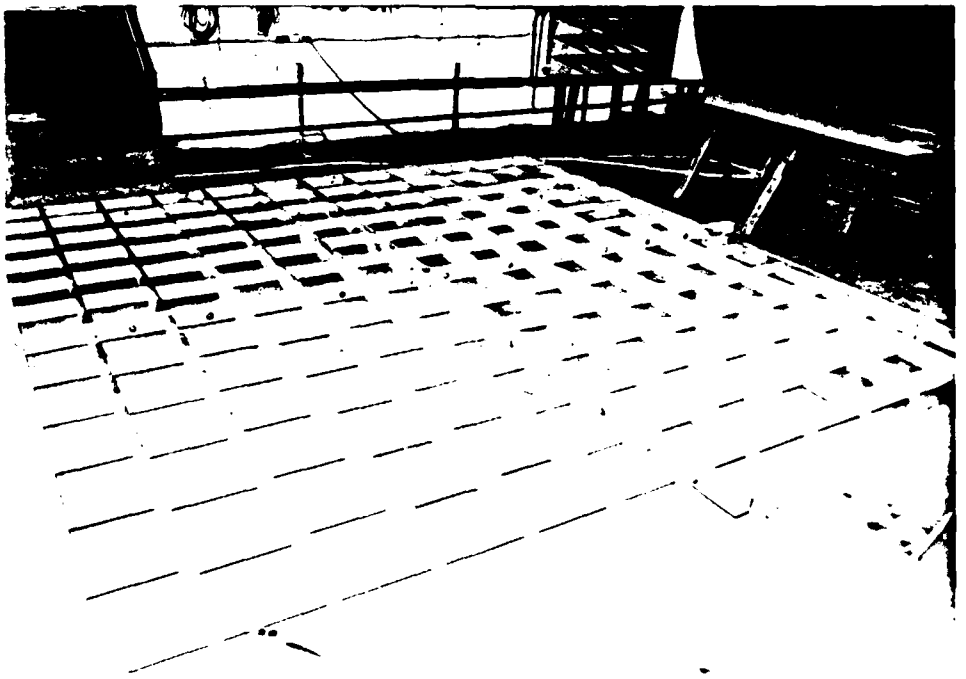

Fig. 2c.

and by covering all wooden surfaces with a minimum of 3 coats of polyester resin. In addition, the edges of all plywood panels were coated with polyester resin before attachment to the framework. This scheme was not successful, apparently because the polyester resin coating was fractured by movement within the structure under load of water. Inspection revealed water penetration into the plywood, particularly around nail and screw heads (even though the resin coating had been "built up" in these places) and along the manufacturer's lamination seams of the plywood. The actual amount of water lost due to leakage was insignificant but it was feared that continued seepage into the plywood would cause delamination and render the tank unusable.

An attempt was made to remedy the seepage problem by covering the "trouble spots" with fiberglass cloth submerged in polyester resin. A subsequent test revealed that, under load, water penetrated the cloth also, even though the cloth was under several layers of polyester resin. At this point, consultation with the technical representatives for a number of coating manufacturers indicated that a plywood tank of this size probably could not be made entirely watertight using ordinary coatings (varnishes, resins, etc.). The decision was then made to procure a vinyl liner of the type used in small swimming pools. A 25-mil vinyl liner is being fabricated, and delivery is expected presently.

During the tests for watertight integrity, it was determined that the tank could be filled to full capacity (approximately 26000 l) in less than one hour. This corresponds to a water level change of approximately 2.5 cm to 3 cm per minute.

Filling is accomplished using a 2-in fire hose attached to the high-capacity water supply (Fig. 3). The original design incorporated a 2-in deck drain which permitted draining within 1½ hours; however, installation of the vinyl liner will require the use of 1½-in drains. The draining rate with the 1½-in drain is estimated to be 0.5 cm to 0.8 cm water level per minute. These rates for changing water level are felt to be entirely adequate for conducting the tests proposed.

Slotted Line Apparatus. References [1] and [2] report favorable results in measuring the electrical properties of water (ε_r and σ) by means of a slotted X-band waveguide apparatus. For this project, a similar apparatus has been constructed from WR137(RG-50/U) waveguide, which is conservatively expected to provide an operating band for dominant (TE_{10}) mode from 650 to 900 Mhz when filled with water. This apparatus is depicted in Fig. 4. At 650 Mhz, the "infinite" section is approximately 35λ in length. Major components were obtained from salvage or purchased under cost-sharing.

In order to provide for measurement of water properties at lower frequencies than can be propagated in WR137 waveguide and to have available independently measured data for corroboration, a more elaborate slotted coaxial line has been designed and is under construction. Illustrations of the design details and photographs of completed parts of the apparatus are included in Fig. 5. The coaxial line is expected to permit reliable measurements at frequencies as low as 500 Mhz, at which the length of the "infinite" line is approximately 20λ. Introduction of salt into the water may increase losses along the "infinite" line to the point where frequencies as low

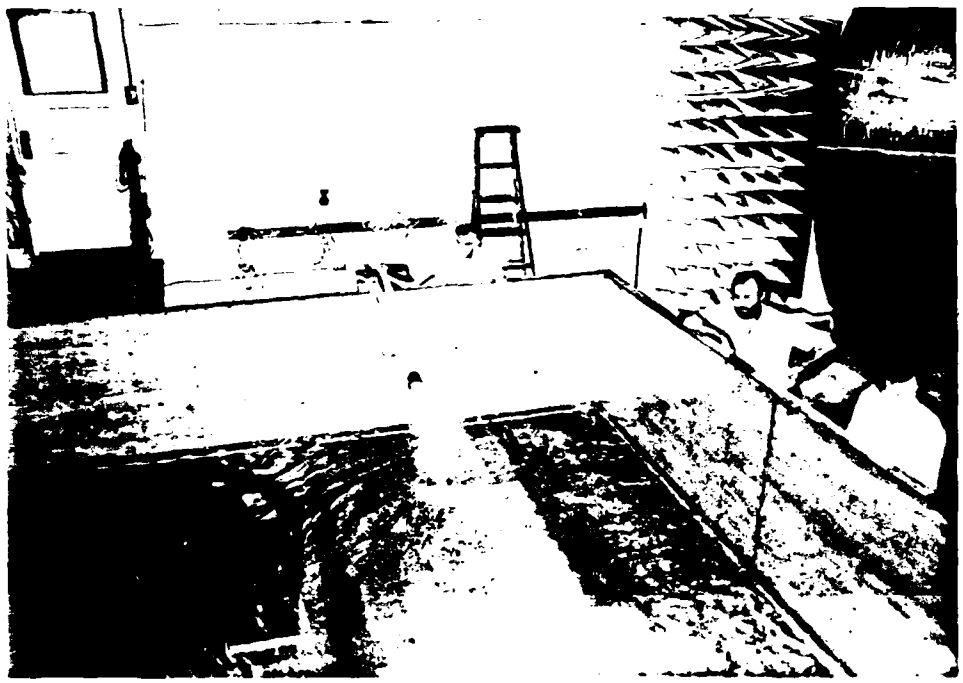

Fig. 3. Filling water tank.

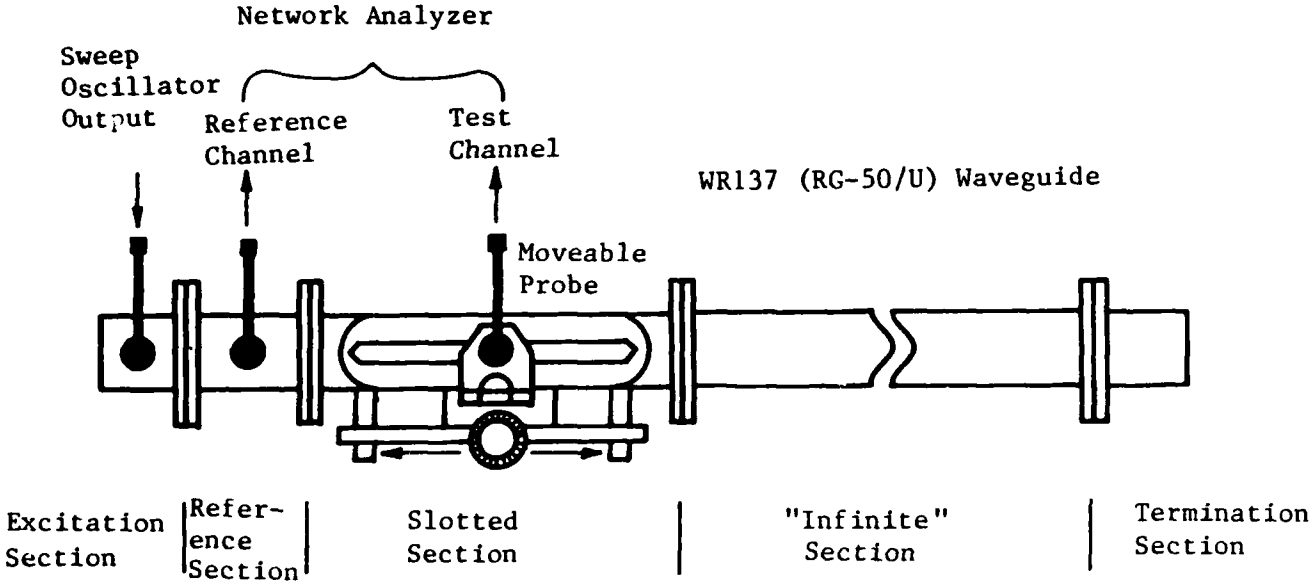

Fig. 4(a). Schematic of slotted waveguide apparatus.

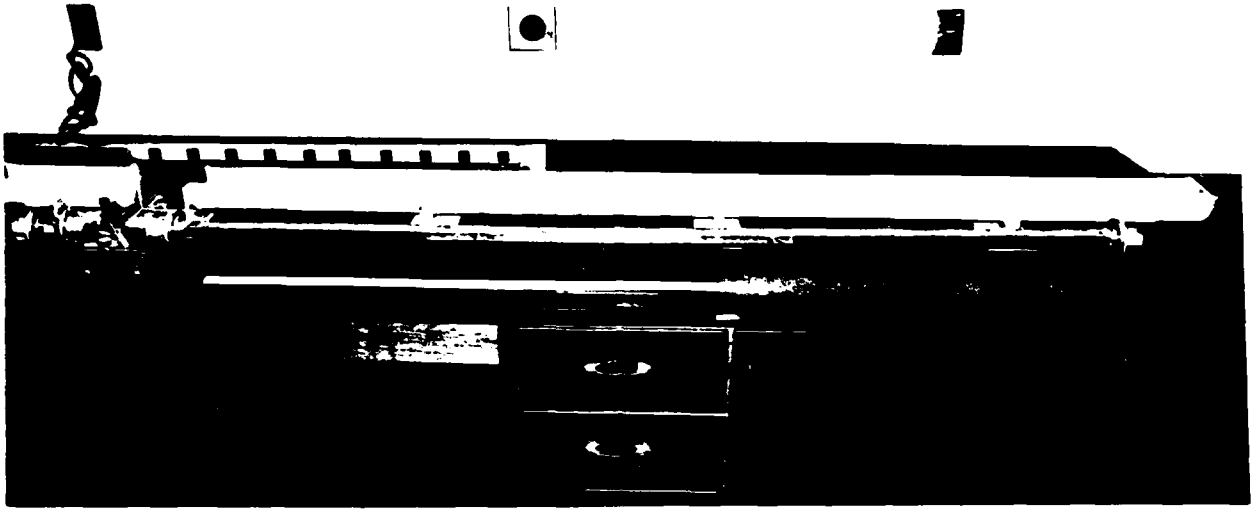

Fig. 4(b). Slotted waveguide apparatus with water trough in background.

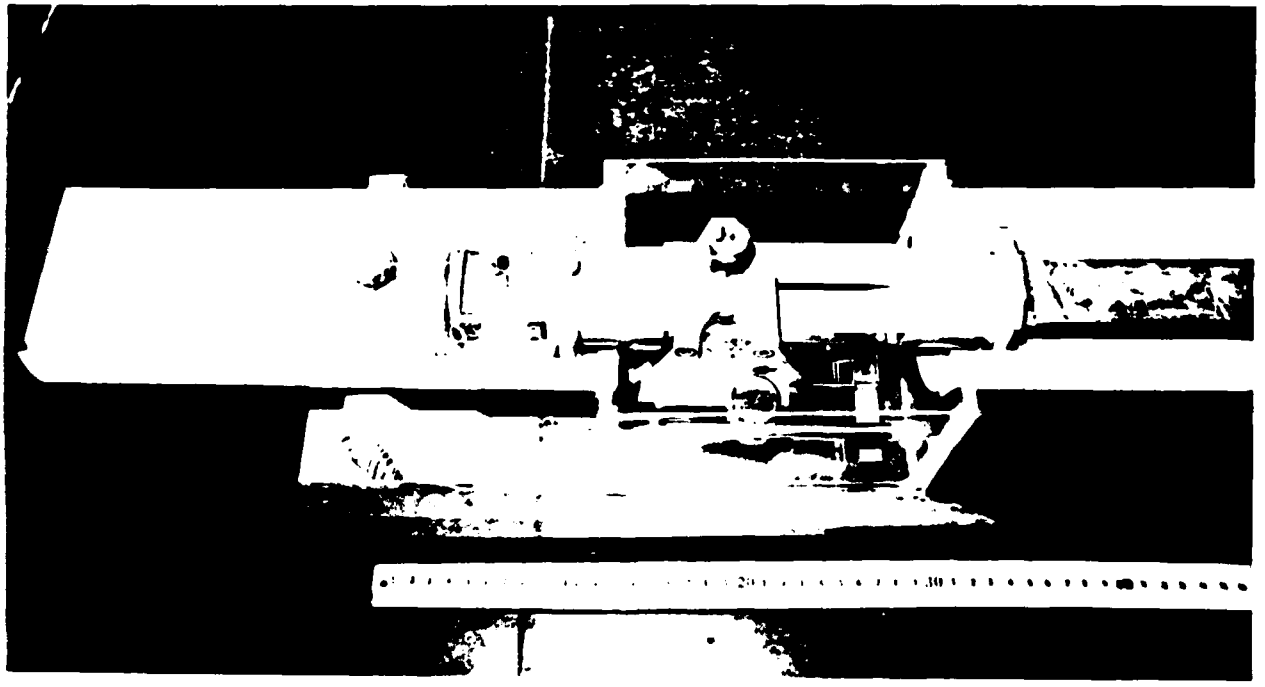

Fig. 4(c). Slotted section in position for submersion.

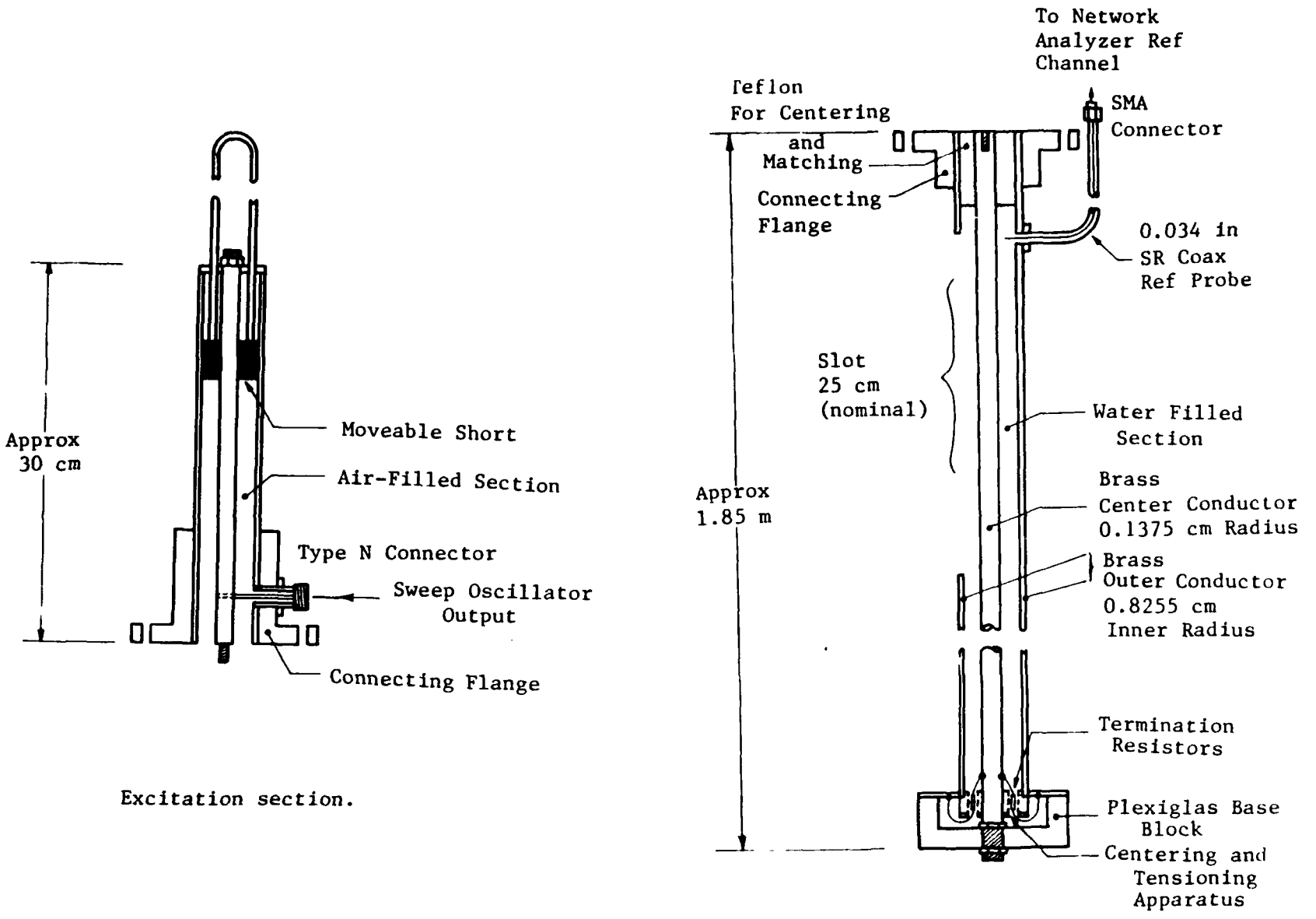

Fig. 5(a). Slotted coaxial line.

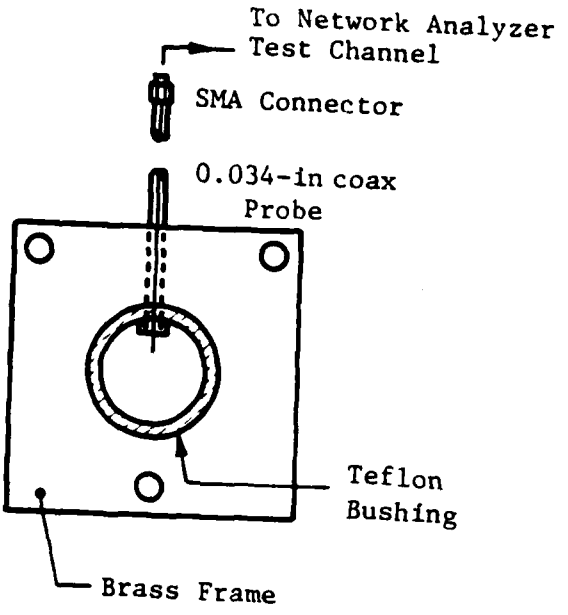

Fig. 5(b). Sliding probe (end view).

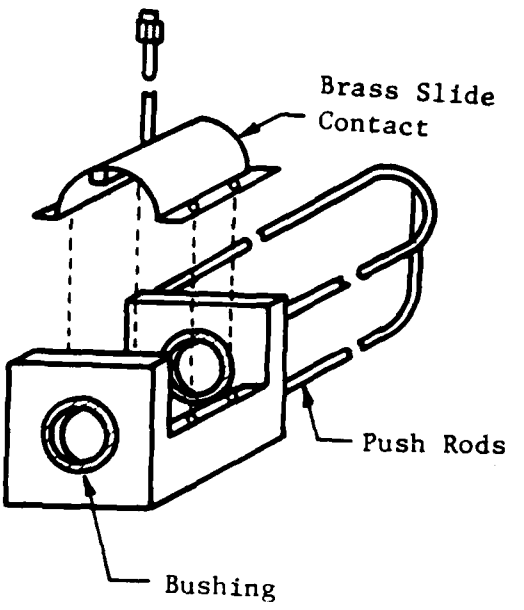

Fig. 5(c). Sliding probe (exploded view).

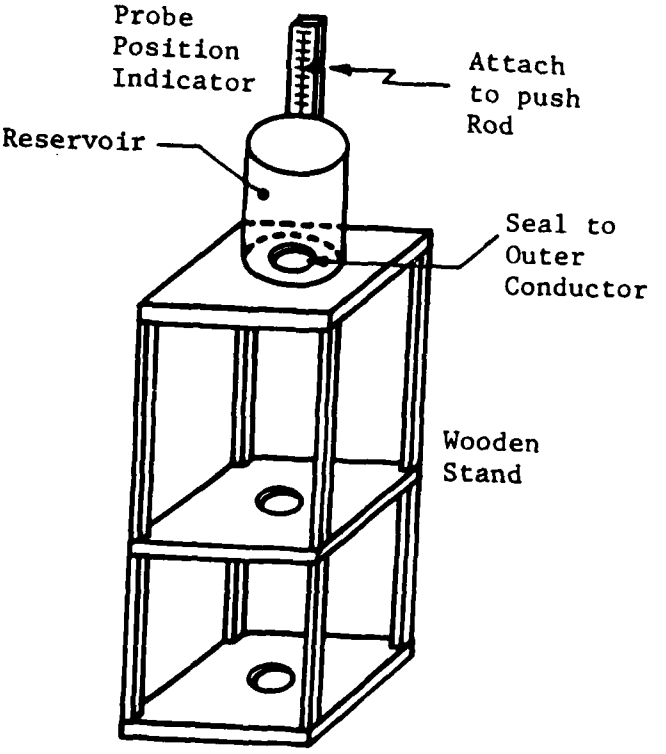

Fig. 5(d). Slotted coax apparatus water reservoir.

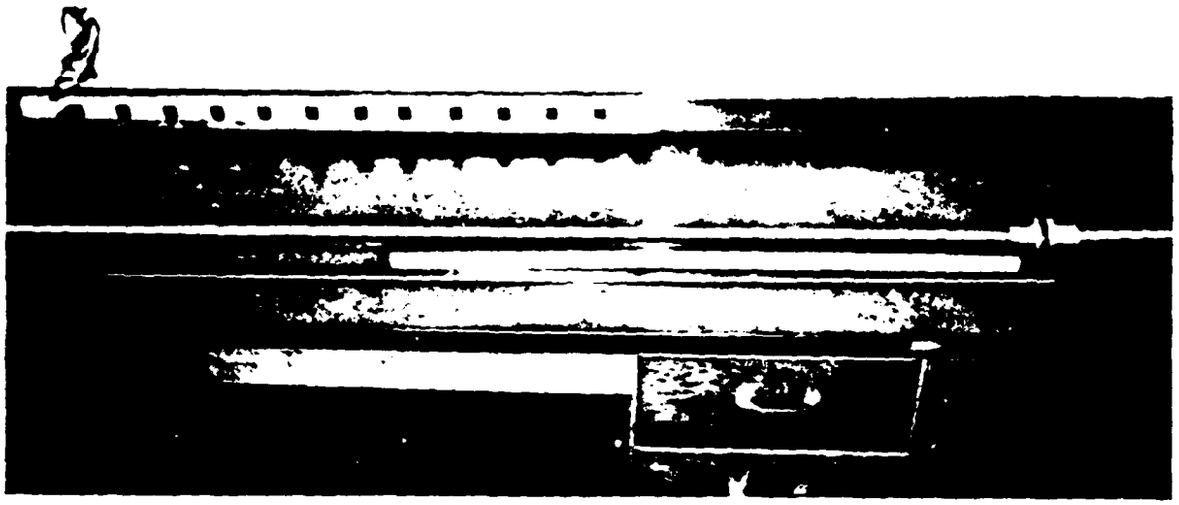

Fig. 5(e). Slotted coax; center conductor in foreground.

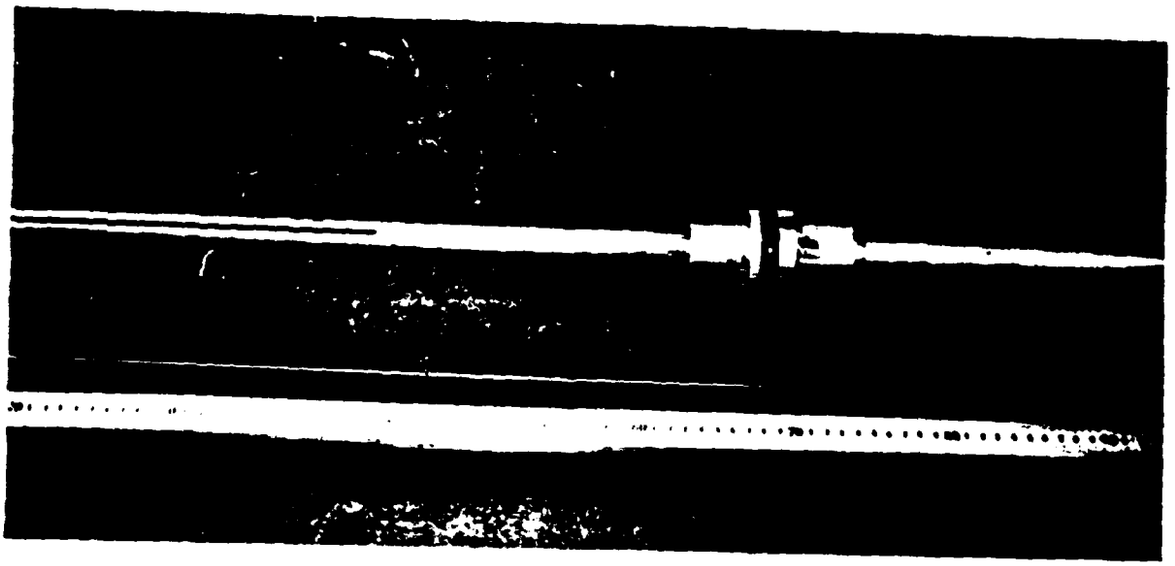

Fig. 5(f). Slotted coax; close-up of slot and connector flanges.

as 300 Mhz may be used.

For the TEM propagation mode of a coaxial line, the propagation constant k is given as

$$k = j\omega\sqrt{\mu\varepsilon} = \beta - j\alpha$$

where

$$\varepsilon = \varepsilon_0\varepsilon_r - j\frac{\sigma}{\omega}$$

and ω, μ, ε and σ have the usual definitions. To determine ε_r and σ for the water dielectric, one proceeds as outlined in references [1] and [2] to calculate α and β from measured ratios of the E-field at various positions along the line to the E-field at some reference position on the line. Since

$$k^2 = (\beta - j\alpha)^2 = (\beta^2 - \alpha^2) - j2\alpha\beta$$

and

$$k^2 = \omega^2\mu\varepsilon = \omega^2\mu\varepsilon_0\varepsilon_r - j\omega\mu\sigma \ ,$$

then

$$\varepsilon_r = \frac{\beta^2 - \alpha^2}{\omega^2\mu_0\varepsilon_0} = \lambda_0^{\,2}\ (\beta^2 - \alpha^2)$$

and

$$\sigma = \frac{2\alpha\beta}{\omega\mu_0} = \frac{\lambda_0}{\eta_0}\left(\frac{\alpha\beta}{\pi}\right) \ .$$

Each water sample is to be analyzed using both slotted lines. It is expected that the results will serve as mutual confirmation of the validity of the techniques.

Test Antennas. The test antennas to be used in PHASE II are sleeve-fed monopoles for which the radiating structure is of circular cross-section and sufficiently small in radius to permit thin-wire analysis. This

type of antenna, when mounted above a ground plane, was analyzed by Butler and Harrison [3] in 1971 using a method of moments (MOM) solution to the Hallen's equation. As part of this project, a MOM solution to the Pocklington's equation for the sleeve-fed monopole has been developed. This work was done, first, to gain a better understanding of these antennas, second, to obtain baseline data from which to estimate behavior of the antennas above a nonideal conducting plane, and, third, to reflect improvements in the MOM technique. Further, since the performance of each antenna is being verified by measurements above a ground plane, the Pocklington code is used to verify antenna performance. Results, to this point, have been entirely consistent.

For each experiment, three antennas have been constructed, one of 0.108-cm radius, a second of 0.179-cm radius and a third of 0.318-cm radius. Current plans are to conduct some otherwise identical tests using each antenna. If the results obtained with the thinner antennas support the thin-wire assumptions for the 0.318-cm antenna, as is expected, then the preponderance of experimentation will be conducted using the more rigid 0.318-cm antenna.

The sleeve-fed monopole antennas have been fabricated and are shown in Fig. 6. Note that the 0.318-cm antenna has detachable extensions to provide a variety of antenna heights from 6 cm to 25 cm above the source gap. The other two antennas have fixed heights of 25 cm above source gap. All antennas have a sleeve length of approximately 90 cm. These antennas are constructed from 50-ohm semi-rigid coaxial cable with unjacketed copper outer conductor. The 0.108-cm radius antenna

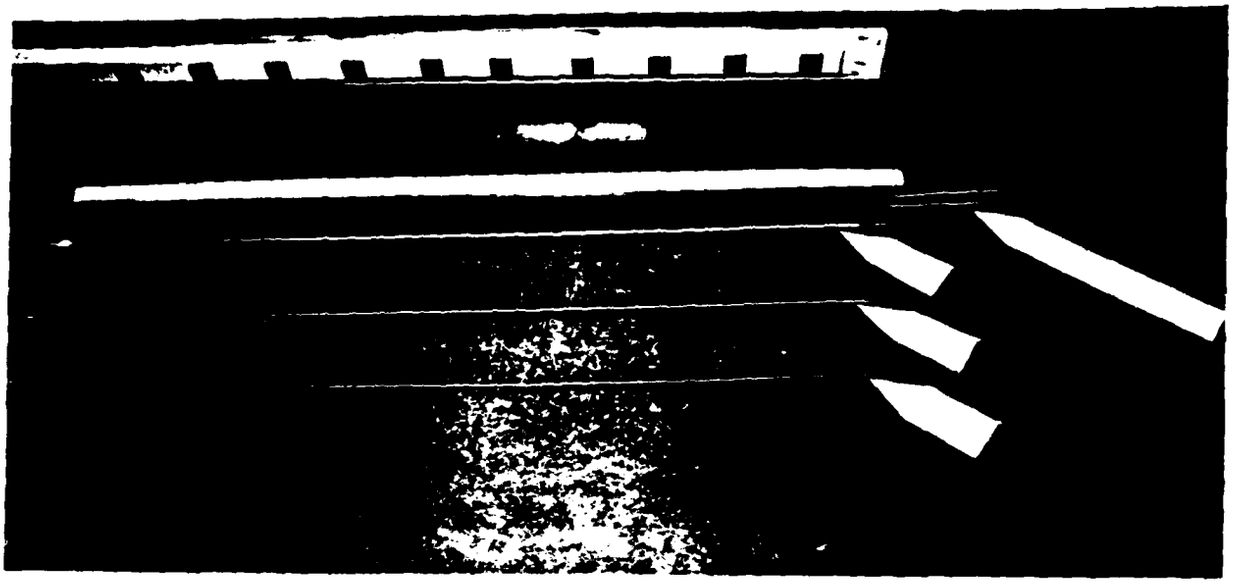

Fig. 6(a). Antennas.

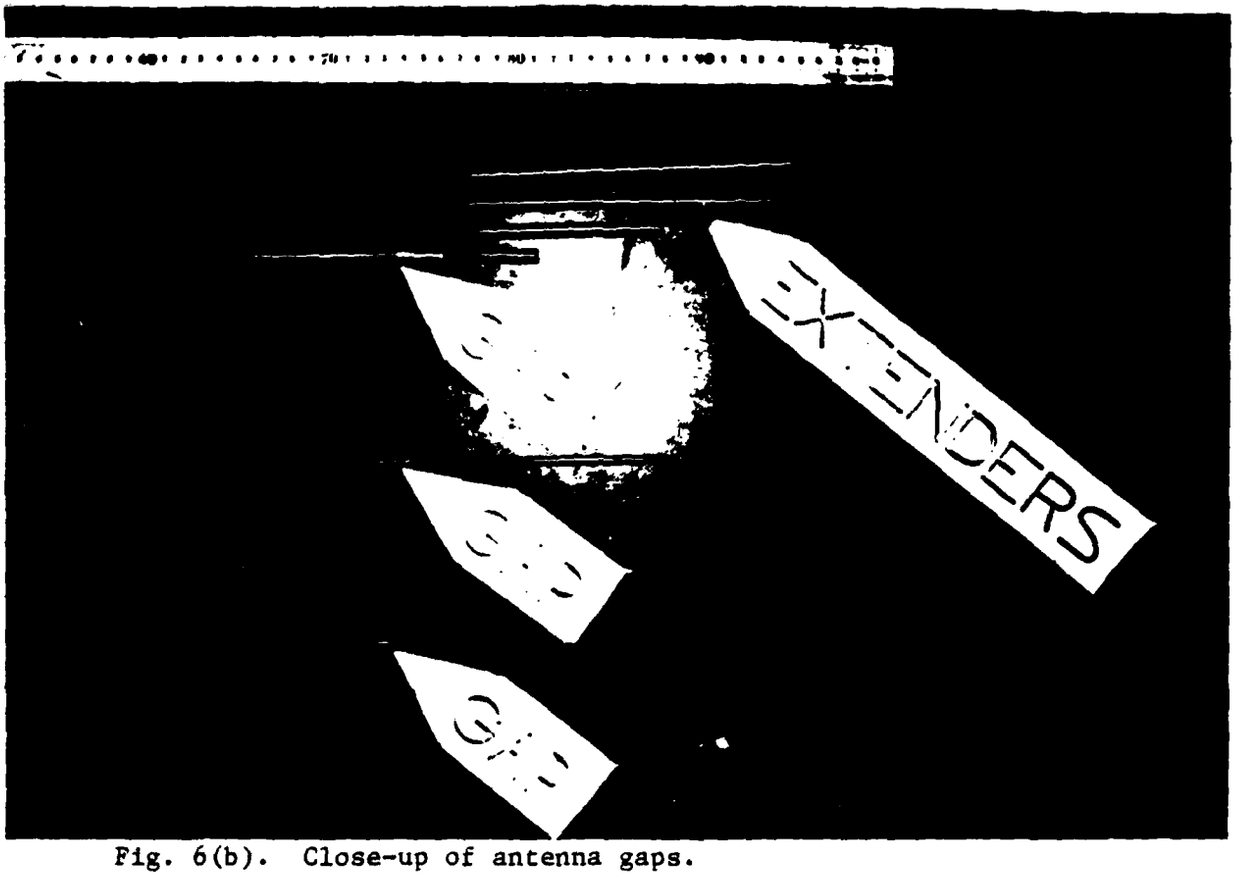

Fig. 6(b). Close-up of antenna gaps.

is fabricated from 0.085-in coax, the 0.179-cm radius from 0.141-in coax, and the 0.318-cm radius from 0.250-in coax. The radiating structure above the source gap is a hollow tube obtained by removing the dielectric and the inner conductor from a section of coax. The end nearest the gap is plugged with conductor, only to a depth sufficient to permit soldering to the center conductor from the feed sleeve. With care in fabrication and handling, it is possible to have gap widths of approximately 0.5 mm, or about one-half radii for the thinnest (0.108-cm) antenna to one-sixth radii for the thickest (0.318-cm) antenna. The driving point is a male SMA connector attached directly to the feed sleeve.

Straight and bent-wire monopole antennas are required for PHASE III; materials for these antennas have been procured and the antennas will be fabricated and tested as needed. These antennas are also to be constructed from 50-ohm semi-rigid coaxial cable with a male SMA connector at the driving point. The outer conductor will be terminated flush with the front side of the conducting screen and the center conductor will be extended to form the radiating element. The 0.085-, 0.141- and 0.250-in coax will provide radiating elements with radii of 0.0255, 0.0455 and 0.0815 cm respectively.

Ground Plane. A conducting screen is to be used during PHASE III experiments. The design specifies heavy-gauge aluminum to be clamped along the top edge and suspended as a curtain along and just inside one wall of the water tank. This design will allow the aluminum to be raised from the tank when not in use. A source of salvaged 1/8-in aluminum panels nominally 8 ft by 16 ft, but damaged along the edges,

has been located, and procurement is in process. Two of these panels will be trimmed and seamed to form a ground plane approximately 4.5 m (14 ft - 6 in) wide by 3 m (10 ft) high.

Instrumentation. The basic instrument for measurement of both the E-field ratios in the slotted line apparatus and the antenna driving point impedances is the Hewlett-Packard 8410A Network Analyzer System. System diagrams for both types of measurements are shown in Fig. 7. The measurements process has been automated through the use of a Tektronix 4052 Computer/Controller. Frequency stability is maintained by a loop containing Hewlett-Packard 5435A Electronic Counter. An Amplifier Research Model 1W1000 Broadband Power Amplifier has been ordered. Incorporation of this amplifier with its nominal 1 W output is expected to boost power levels adequately to offset the mismatch between air-filled and water-filled regions in the slotted apparatus and to accomodate the extended lengths of antenna feed line required when the driving point is below the water surface.

PHASE II - Experiments Involving Antenna Driving Points Below Water Surface

Antenna Configurations and Experiment Geometry. In this phase of the experiment, the antenna configuration is a straight-tube, sleeve-fed monopole positioned with its cylindrical axis normal to the air/water interface and with the source gap in air (see Fig. 8(a)). The driving point is located as near to the bottom of the tank as is practical. The water level will be varied to provide different values of gap height (g), ranging from as small as practical to $\lambda/2$. This experiment will be repeated for all three antennas (a = 0.108 cm,

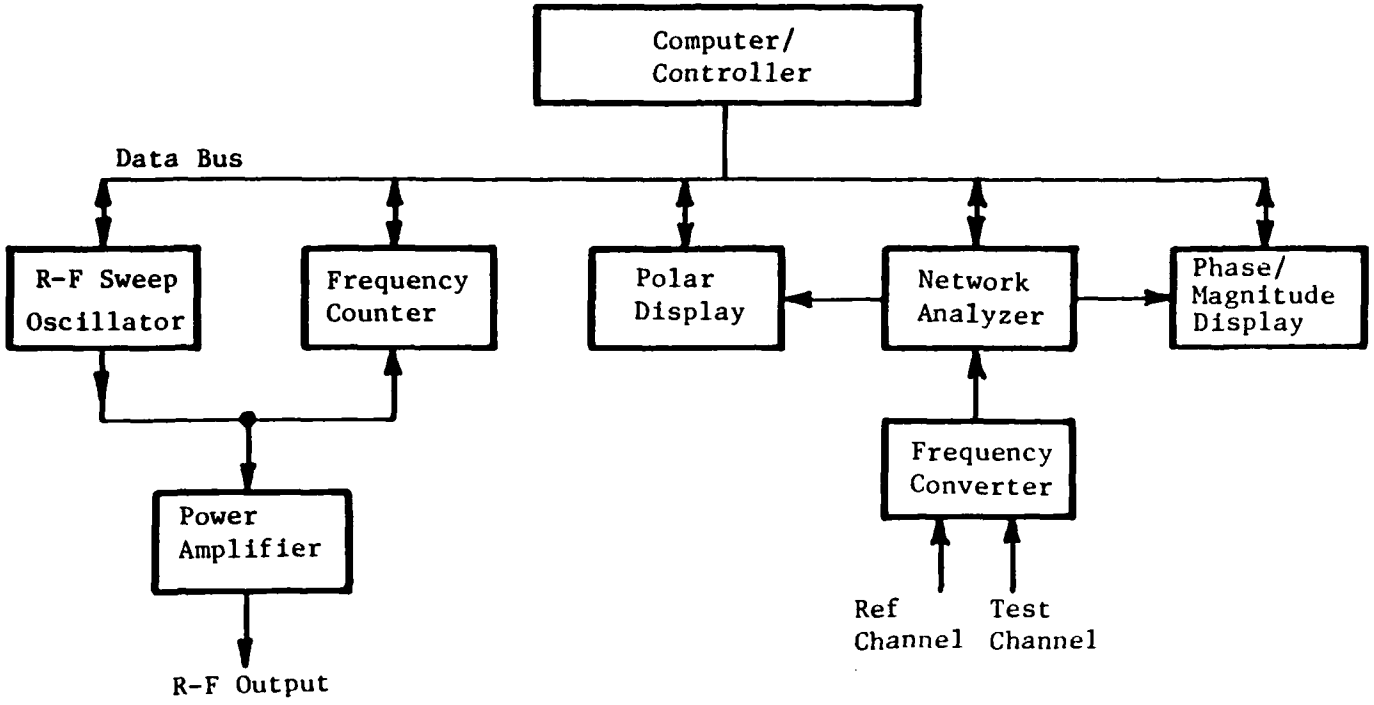

Fig. 7(a). Instrumentation for E-field ratio measurements.

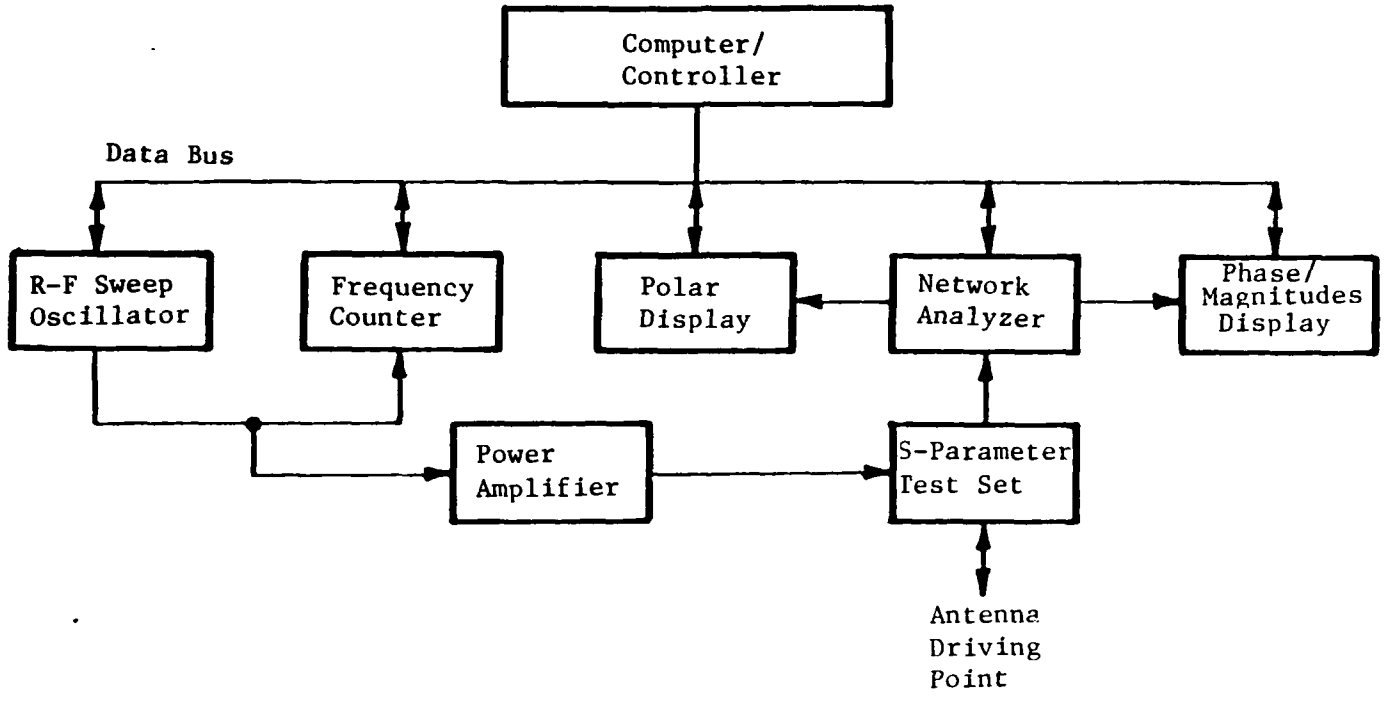

Fig. 7(b). Instrumentation for antenna impedance measurements.

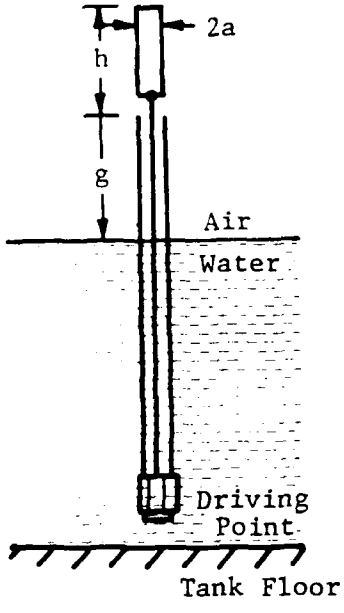

Fig. 8(a). Antenna configuration for PHASE II measurements.

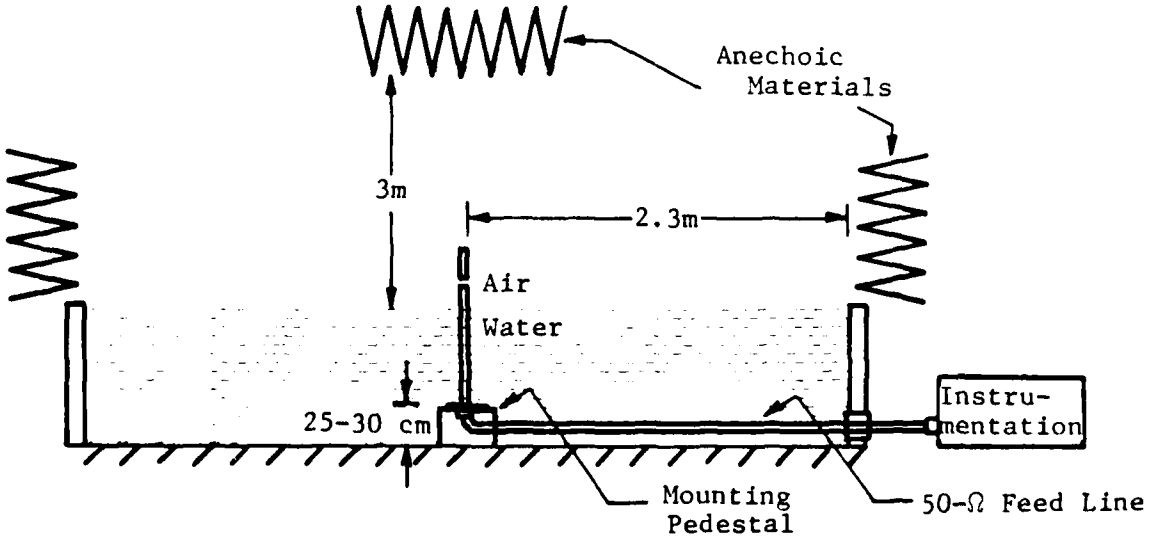

Fig. 8(b). Equipment layout for PHASE II measurements.

a = 0.179 cm and a = 0.318 cm). For the 0.318-cm antenna, extenders will be used to provide different lengths of radiating structure (h) above the source gap. If necessary, these experiments can be repeated for the thinner antennas by successively "snipping" the hollow tube above the source gap.

Equipment Layout and Procedural Considerations. The antenna is to be mounted to a wooden pedestal such that the driving point will be located 25-30 cm above the tank floor. This distance above the floor is dictated by the minimum bend radius of the feed line, the length of connectors and adapter, and the requirement to encase the connection in a water-proof seal. The feed line is a ½-in Spirafil coax specified to have losses of 0.05 to 0.08 db/m in the frequency range of interest. Type N connectors are required with the Spirafil coax; therefore an adapter is required to accommodate the SMA connector at the antenna driving point. The length of feed line will be minimized by having the coax exit the tank wall at floor level and by placing the S-parameter test set of the network analyzer as close as possible to the tank wall. The calibration technique to be used with the network analyzer will establish an electrical reference plane several centimeters above the physical driving point of the antenna and will thus eliminate connector discontinuities from the final data.

Anechoic materials will be placed around and above the tank at a range of 2-3 meters from the antenna. The antenna will be located slightly away from tank center to avoid any degradation of the experiment due to in-phase reflections from the surroundings. Salt will be added to the water to assure that the water is sufficiently

lossy to cause the currents on the outside of the sleeve to decay, and hence cause the sleeve to appear infinite in length.

A sight gauge located outside the tank will permit accurate determination of water level. In addition, phenomena such as capillary action of the water on the walls of the thin antennas will be considered.

PHASE III - Experiments Involving Antenna Driving Points Above Water Surface, but Behind a Conducting Screen

Antenna Configurations and Experiment Geometry. In this phase of the experiment, the antenna configuration may be a straight- or bent-wire monopole positioned above the air/water interface. The driving point will be located behind a conducting screen which intersects the water surface at a right angle (see Fig. 9(a)). The water level will be varied to provide different separations (h) between the antenna and the water surface. In some cases h will be made as small as practical, which means that in experiments with bent-wire antennas, h' may be below the water surface. As in PHASE II, some experiments will be repeated with antennas of all three radii in order to validate the thin-wire assumption.

Equipment Layout and Procedural Considerations. The conducting screen will be suspended as near as practical to one wall of the tank and lowered until the bottom edge is as near as practical to the tank floor. The antenna mount will be located as close as practical to the top edge of the tank wall and offset slightly from the horizontal center of the screen. The configuration provides screen ranges of approximately 4.5λ horizontally and 3.5λ vertically in air, and

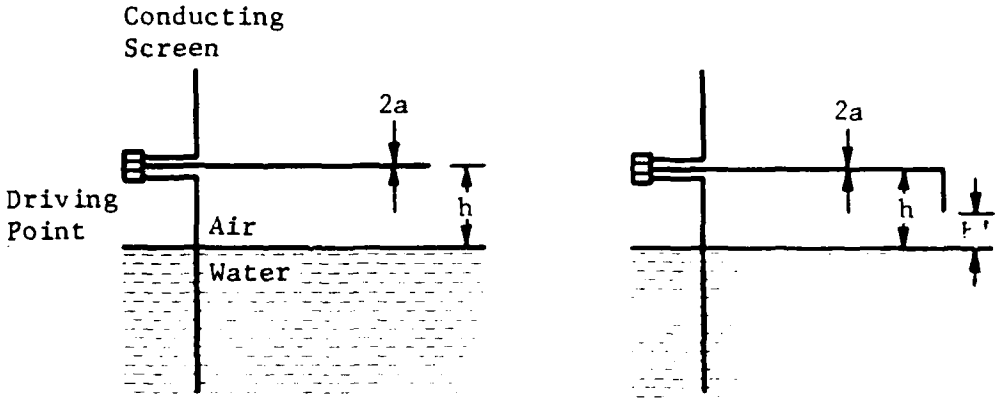

Fig. 9(a). Antenna configurations for PHASE III measurements.

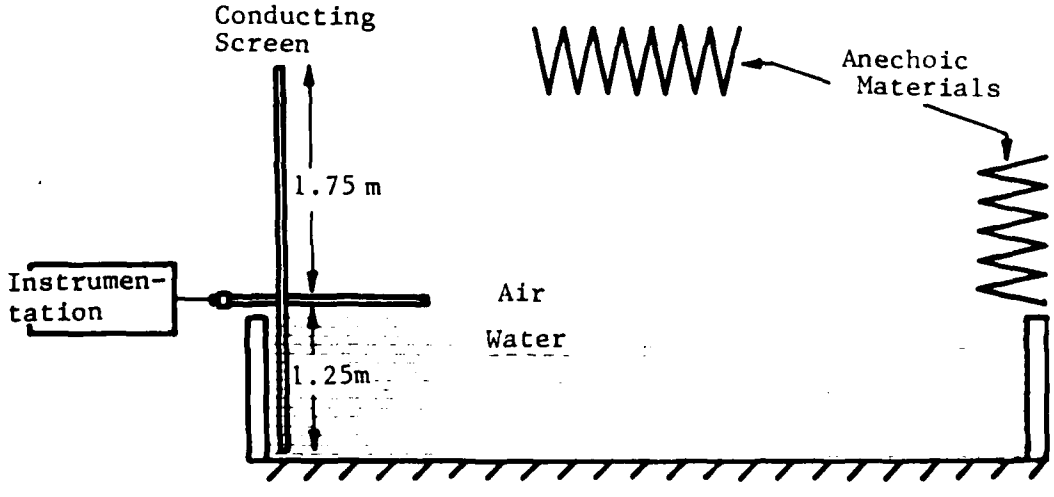

Fig. 9(b). Equipment layout for PHASE III measurements.

approximately 40λ horizontally and 20λ vertically in water, at 600 Mhz. Greater screen ranges in air would be desirable, but are not practical at the frequencies of interest.

The antennas will be constructed so that the driving point is as close as practical to the rear side of the conducting screen. The network analyzer will be connected directly to the SMA connector at the antenna driving point. Again, the calibration technique will serve to eliminate connector discontinuities.

As in the PHASE II experiments, anechoic materials will be placed around and above the tank. Fresh water may be used in these experiments because increased water losses are not required.

REFERENCES

1. Butler, C. M., et. al., "Experimental Investigation of a Monopole in a Lossy Medium," Final Report N66001-81-M-5991, Naval Ocean Systems Center, San Diego, CA 92152; September, 1981.

2. Butler, C. M., et. al., "Experimental Investigation of a Wire Antenna Above a Lossy Medium," Final Report N66001-81-0-021 ORS, Naval Ocean Systems Center, San Diego, CA 92152; September, 1981.

3. Butler, C. M. and M. G. Harrison, "Analysis of the Sleeve Monopole Antenna," Proceedings of the 9th Annual (1971) IEEE Region III Convention, No. 71 C 16-REG 3, pp. 303-308; April, 1971.

END
DATE
FILMED

Jan. 7, 1983